Master's Thesis

Unveiling Battery Pack Failure Modes and Optimizing Test Bench Performance

In partial fulfillment of the requirements for the degree
Master of Science
at the TUM School of Engineering and Design
of the Technical University of Munich.

Advisor

Prof. Dr. rer. nat. Thomas Hamacher
Prashant Pant
Chair of Renewable and Sustainable Energy Systems

Submitted by

Marco Rondoni
Lichtenbergstraße 4
85748 Garching
+39 3898489445

Submitted on Munich, February

Abstract

The rapid expansion of electric vehicles (EVs) demands robust and efficient battery testing to ensure safety, reliability, and cost-effectiveness. This thesis employs the Physics of Failure (PoF) approach to investigate failure modes in lithium-ion battery packs, identifying key thermal, mechanical, and electrochemical stressors that lead to degradation. By integrating endurance driving profiles with Accelerated Life Testing (ALT), the study refines battery testing using the Table of Damage approach. The goal is to eliminate redundant tests, reduce costs, and accelerate validation processes while maintaining test accuracy. The findings contribute to the development of more reliable and efficient battery testing frameworks, directly impacting EV innovation and sustainability.

keywords - **Physics of Failure (PoF), Table of Damage, Battery Testing, Accelerated Life Testing (ALT)**

Statement of Academic Integrity

I,

Last name: Rondoni
First name: Marco
ID No.: 03749020

hereby confirm that the attached thesis,

Unveiling Battery Pack Failure Modes and Optimizing Test Bench Performance

was written independently by me without the use of any sources or aids beyond those cited, and all passages and ideas taken from other sources are indicated in the text and given the corresponding citation.
I confirm to respect the “Code of Conduct for Safeguarding Good Academic Practice and Procedures in Cases of Academic Misconduct at Technische Universität München, 2015”, as can be read on the website of the Equal Opportunity Office of TUM.
Tools provided by the chair and its staff, such as models or programs, are also listed. These tools are property of the institute or of the individual staff member. I will not use them for any work beyond the attached thesis or make them available to third parties.

I agree to the further use of my work and its results (including programs produced and methods used) for research and instructional purposes.

I have not previously submitted this thesis for academic credit.

Munich, February Marco Rondoni

Declaration for the Transfer of the Thesis

I agree to the transfer of this thesis to:

- Students currently or in future writing their thesis at the chair:
  - ☒ Flat rate by employees
  - ☐ Only after particular prior consultation.
- Present or future employees at the chair
  - ☒ Flat rate by employees
  - ☐ Only after particular prior consultation.

My copyright and personal right of use remain unaffected.

Munich, February 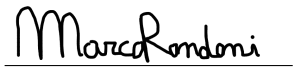

Contents

Chapter 1

Introduction

Lithium-ion batteries (LIBs) have become a focal point of interest due to their exceptional ability to store energy efficiently and support environmentally sustainable solutions. Their applications extend beyond portable devices like laptops and smartphones to powering electric, hybrid, and electric vehicles, demonstrating their critical role in advancing contemporary energy technologies [1, 2]. However, as the demand for LIBs in automotive applications grows, ensuring their reliability, safety, and performance under real-world conditions has become increasingly important. The complexity of modern battery packs presents challenges in predicting failure modes, optimizing testing strategies, and improving overall durability. These challenges necessitate rigorous testing protocols, regulatory compliance, and innovative methodologies to accelerate battery testing while maintaining accuracy and relevance. This thesis focuses on investigating failure modes in automotive battery packs using the Physics of Failure (PoF) approach. By employing vehicle endurance driving profiles and accelerated stress profiles, the research aims to establish a more efficient testing methodology. The study integrates the Table of Damage approach to assess battery degradation under Accelerated Life Testing (ALT), helping to identify key stress factors that contribute to early failures.

A significant goal of this work is to optimize battery performance testing by eliminating redundant or non-informative tests while maintaining reliability. By refining the testing framework, the study aims to bridge the gap between real-world driving conditions and laboratory testing, providing insights that can enhance the design and validation of lithium-ion battery systems for electric vehicles.

This thesis will contribute to the broader field of battery reliability assessment by offering a structured methodology that can accelerate testing without compromising the accuracy of failure predictions. The findings will be relevant to manufacturers, regulatory bodies, and researchers looking to improve the safety and efficiency of battery testing practices.

1.1 Battery cells structure & working principle

LIBs comprise four key components: the cathode, anode, separator, and electrolyte [3]. The cathode and anode are responsible for energy storage and release, while the separator prevents internal short circuits by keeping the electrodes apart but

allowing the passage of lithium ions (Li^+). The electrolyte acts as the medium through which ions move.

The electrochemical reactions in a typical LIB depend on the cathode material. The operating principle of a typical LIBs, using a $LiNiMnCoO_2$ (NMC) cathode and graphite anode, involves the movement of Li^+ ions during charging and discharging. During charging, Li^+ ions de-intercalate from the cathode, travel through the electrolyte and separator, and intercalate into the anode. Electrons flow through the external circuit to maintain charge balance. The process reverses during discharge. The reactions are as follows:

$$\begin{aligned} \text{Cathode:} \quad & LiNiMnCoO_2 \leftrightharpoons Li_{(1-x)}NiMnCoO_2 + xLi^+ + xe^- \\ \text{Anode:} \quad & 6C + xLi^+ + xe^- \leftrightharpoons Li_xC_6 \\ \text{Overall Reaction:} \quad & LiNiMnCoO_2 + 6C \leftrightharpoons Li_{(1-x)}NiMnCoO_2 + Li_xC_6 \end{aligned}$$

For a $LiCoO_2$ (LCO) cathode, the charge and discharge processes involve the following reactions:

$$\begin{aligned} \text{Cathode:} \quad & LiCoO_2 \leftrightharpoons Li_{(1-x)}CoO_2 + xLi^+ + xe^- \\ \text{Anode:} \quad & 6C + xLi^+ + xe^- \leftrightharpoons Li_xC_6 \\ \text{Overall Reaction:} \quad & LiCoO_2 + 6C \leftrightharpoons Li_{(1-x)}CoO_2 + Li_xC_6 \end{aligned}$$

Heat is a natural byproduct of these reactions, but inefficient dissipation during certain states can cause overheating, compromising battery safety [4].

LIBs are available in four main formats: cylindrical, prismatic, pouch, and coin cells [5]. Cylindrical cells, such as those used in Tesla vehicles, feature robust metallic casings and effective heat dissipation due to the spacing between cells. Prismatic cells, common in BYD vehicles, offer higher capacity but are more prone to heat management issues. Pouch cells are lightweight and flexible in matching a specific device shape but have less durable casings, making them vulnerable to deformation under stress. From a safety perspective, cylindrical cells generally exhibit the lowest risks, followed by pouch and prismatic cells [6].

In practical applications, large battery packs are assembled by combining hundreds or thousands of cells in series and parallel configurations to achieve the desired voltage and capacity [7]. Tesla electric vehicles, for instance, rely on approximately 7,000 cylindrical cells to achieve a total capacity of 85 kWh and a voltage of 400 V. While this large-scale configuration enables impressive performance, it also introduces significant engineering challenges in ensuring both safety and reliability. Failures in individual components, such as separators or electrolytes, can severely compromise battery performance and safety. During operation, electrochemical reactions generate heat, and inadequate heat management can exacerbate the risks, particularly if separator failure occurs. This can lead to uncontrolled chain reactions fueled by the electrolyte, highlighting the critical need to understand and mitigate failure mechanisms to enhance the overall safety and resilience of battery systems [6].

1.2 Types of battery cells technologies in the market

When comparing different battery technologies, their performance is often evaluated in terms of volumetric energy density (measured in Wh/L) and gravimetric energy density (measured in Wh/kg). To illustrate this, a Ragone diagram has been included in Figure 1.1. In this diagram, the y-axis represents volumetric energy density (Wh/L), which indicates how much energy a battery can store per unit of volume, while the x-axis represents gravimetric energy density (Wh/kg), showing how much energy is stored per unit of weight. This visual representation highlights the trade-offs between compactness and lightweight efficiency across different battery technologies.

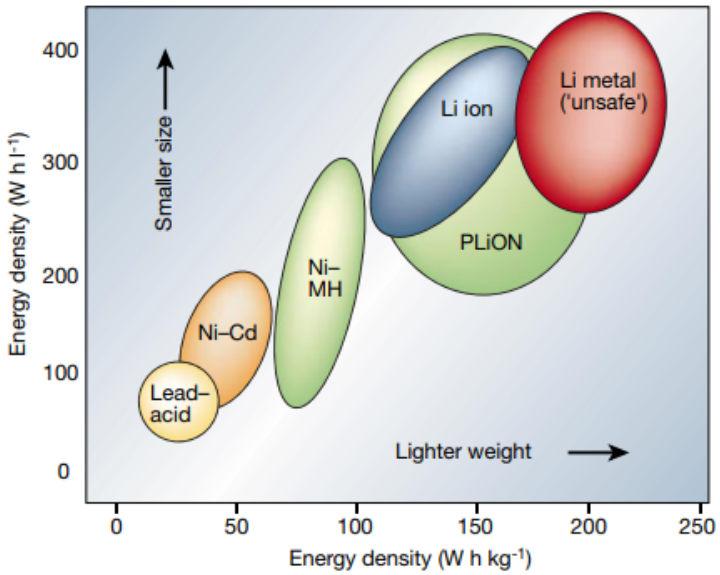

Figure 1.1 Ragone plot of several of the battery technologies used in electric vehicles (EVs) [5].

Lithium-ion (Li-ion) batteries dominate the portable battery market, accounting for 63% of global sales. Their high energy densities make them ideal for modern applications such as portable electronics and electric vehicles. In the Ragone diagram, they appear in the upper-right region, showcasing their strong performance in both volumetric and gravimetric metrics. Nickel–cadmium (Ni–Cd) batteries, which hold 23% of the market, excel in high-power applications like power tools due to their robust design and ability to deliver significant power. Nickel–metal hydride (Ni–MeH) batteries, representing 14% of sales, provide moderate energy density and are often used as a transitional technology between Ni–Cd and Li-ion batteries. Lead–acid (Pb–acid) batteries, on the other hand, are primarily utilized in starting, lighting and ignition (SLI) applications in vehicles and for backup power systems [5]. While they are affordable and benefit from a well-established recycling process, their relatively low energy densities position them at the lower-left corner of the Ragone diagram, limiting their use in advanced or portable technologies.

The included Ragone diagram provides a clear overview of these differences, illustrating the strengths and weaknesses of each battery type. It underscores the

importance of ongoing innovation in battery technology to meet the evolving needs of diverse applications.

In the following, two types of lithium-ion cell chemistries are discussed, respecivelly Lithium Cobalt Oxide (LCO) and Lithium Nickel Manganese Cobalt Oxide (NMC), along with their respective strengths and weaknesses. The electrochemical reactions of these chemistries were already introduced in Section 1.1.

The lithium cobalt oxide battery, first developed by Sony in 1991, has become the go-to power source for many personal electronic devices such as laptops, cameras, and tablets [8]. This is mainly due to its high energy density, long lifespan, and relatively easy manufacturing process. However, lithium cobalt batteries are highly reactive, resulting in poor thermal stability, which requires careful monitoring during use to ensure safety. Another drawback is the limited availability of cobalt, which makes the batteries both costly and less practical for large-scale applications such as electric vehicles EVs. Despite these challenges, lithium cobalt batteries are still used in high-performance EVs like the Tesla Roadster and the Smart Fortwo Electric Drive, owing to their ability to store a large amount of energy [9].

NMC batteries are known for their high energy density, providing either high specific energy or power. The advantage of NMC comes from combining nickel, which offers high energy but low stability, and manganese, which improves stability by forming a spinel structure, though it provides lower energy [10]. By adjusting the ratio of nickel and manganese, manufacturers can enhance energy density while reducing cobalt content to lower costs. Over time, NMC formulations have advanced from NMC111 to NMC811, which offers higher discharge capacity. This synergy between nickel and manganese has made NMC the most successful and widely used lithium-ion battery chemistry for electric vehicles EVs, including models such as the Nissan Leaf, Chevy Volt, and BMW i3, due to its excellent thermal stability and energy performance [8, 9].

1.3 Present and future roles of battery

In 2019, global sales of EVs, including Battery electric vehicles (BEVs) and Plug-in hybrid electric vehicles (PHEVs), surpassed five million units. BEVs accounted for the majority of these sales, reflecting a growing shift toward fully electric vehicles. The adoption of EVs has accelerated dramatically—what once took five years to achieve, selling one million BEVs, now takes just six months. This rapid growth is largely driven by rising concerns about environmental sustainability and the demand for cleaner, more efficient transportation, particularly in urban areas. To meet this demand, both established automakers and newer companies have introduced a diverse range of EVs with varying features and driving ranges, catering to a broad spectrum of customers [11]. Meanwhile, the focus on electric mobility is expanding beyond road vehicles to include the emerging concept of urban aerial mobility. Electric vertical takeoff and landing (eVTOL) vehicles are becoming a key topic of discussion and are gradually being commercialized to revolutionize urban transportation [12]. As battery-powered transportation gains commercial traction, the need to reduce costs and improve the reliability of battery systems has become more critical than ever.

Chapter 2

Battery Failures

2.1 Battery in automotive

2.1.1 Types of electric power trains

EVs can be classified based on the Powertrain topology. Pure Electric Vehicles (PEV), Series Hybrid Electric Vehicles (Series HEV), Parallel Hybrid Electric Vehicles (Parallel HEV) and Power-split Hybrid Electric Vehicles (PSHEV) are the four main powertrain topologies identified [13].

PEV

PEVs are vehicles exclusively powered by electric energy stored in a battery. Current mass-production PEV include Mitsubishi i-MiEV and Tesla Model S [13]. The powertrain architectures of PEV can be classified based on various factors, such as the number and positioning of electric motors, the type of transmission system, the number of gears, and other key design features. The following analysis focuses on three primary PEV architectures, comparing and examining their differences.

- Type-a: PEV with one EM and no transmission.

  This is the most basic and commonly used layout in nearly all PEV on the market. It closely resembles the architecture of traditional vehicles but eliminates the clutch and transmission. In this design, the battery supplies power directly to the electric motor, which generates torque and transfers it to the differential through a single-speed reduction gear. To save weight and optimize installation space, the propulsion motor, reduction gear, and differential are typically integrated into a single compact unit.

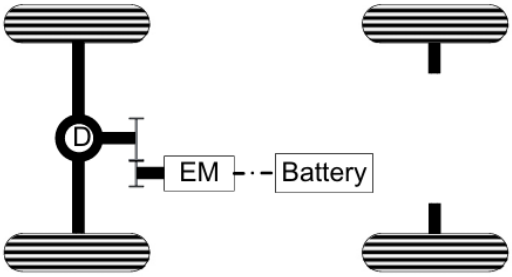

Figure 2.1 PEV with one EM and no transmission from [13].

- Type-b: PEV with one EM and multiple-speed gearbox. This architecture builds upon the Type-A design by adding a multi-speed gearbox between the electric motor (EM) and the differential. This addition addresses some of the key limitations of the Type-A architecture, such as reduced efficiency at high speeds and limited torque delivery in certain scenarios. The gearbox enhances performance by improving acceleration, enabling better energy efficiency across a wider range of speeds, allowing the motor to operate more efficiently while still eliminating the need for a coupling device such as a clutch. Typically, the number of gears in this gearbox does not exceed four [13].

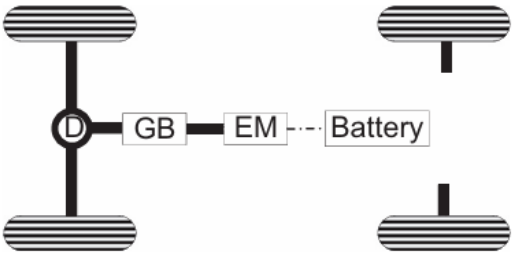

Figure 2.2 PEV with one EM and multiple-speed gearbox from [13].

- Type-c: PEV architecture with more than one EM. Different architectures are designed with more than one EM. In Figure 2.3, the powertrain with four EM is shown. This design uses four "pancake" hub motors, each driving its corresponding wheel. By integrating the motors directly into the wheels, it frees up significant space within the vehicle, creating more room for the battery pack, cargo, and passengers. Another major advantage of this setup is its flexibility. Depending on the configuration, the vehicle can easily operate as front-wheel drive (FWD), rear-wheel drive (RWD), or all-wheel drive (AWD).

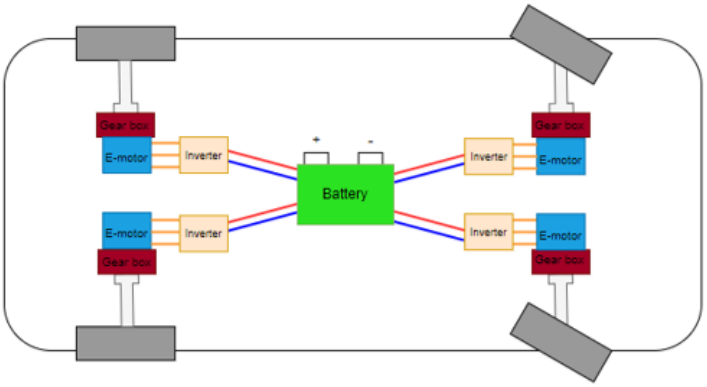

Figure 2.3 PEV with four electric motors

Series HEV

A series hybrid architecture, often found in locomotives, usually consists of a gasoline or diesel engine, an electric generator (EM1), an electric motor (EM2), an energy storage system (ESS), and a vehicle control unit (VCC), among other elements. In this configuration, the engine-generator unit converts fuel's chemical energy into electrical energy, which is then supplied to the traction motor. The motor uses this electricity to produce mechanical power, propelling the vehicle. Various layout options for the Series Hybrid Electric Vehicles (HEV) are possible.

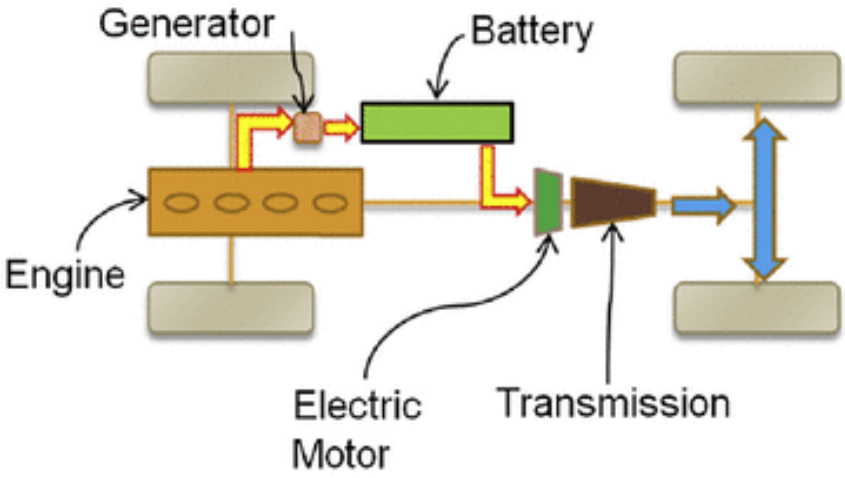

Figure 2.4 Series HEV powertrain scheme from [14]

Parallel HEV

A Parallel HEV powertrain is designed so that the internal combustion engine (ICE) and electric motor (EM) work together, with a fixed speed ratio, to deliver driving torque to the wheels. Both the ICE and the electric motor can operate separately or simultaneously, depending on the driving conditions. The electric motor can assist the engine during acceleration or act as a generator to recharge the battery based

on factors like battery charge and the vehicle's load. The system typically includes the ICE, electric motor, transmission, coupling device, battery pack, and Vehicle Control Unit (VCU). This configuration provides flexibility, optimizing fuel efficiency and performance by adjusting the power sources to meet the demands of various driving scenarios. One of the key benefits of a parallel hybrid is its efficiency across different driving conditions. Since the electric motor and engine can work together or independently, the system can always select the most appropriate power source for the situation. For example, when cruising at higher speeds, the engine can take over to maintain efficiency, while the electric motor can handle lower speeds or assist the engine in situations like acceleration. This combination helps improve fuel economy, especially during highway driving, where the engine is more efficient. However, compared to a series hybrid, there are some trade-offs. In a parallel hybrid, the electric motor and the engine are mechanically connected, meaning the system is more complex. For this reason, the transition between the electric motor and the internal combustion engine in a parallel hybrid can sometimes feel less seamless than in a series hybrid, where the electric motor handles all propulsion, leading to smoother and more continuous power delivery [13].

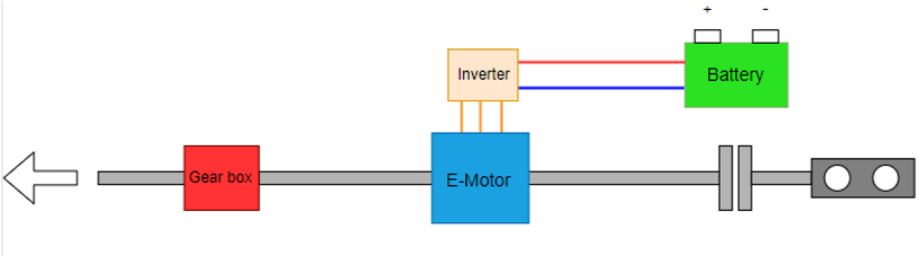

Figure 2.5 Parallel HEV powertrain scheme

PHEVs

A Plug-in Hybrid Electric Vehicles (PHEVs) is a type of hybrid vehicle that combines an electric motor and a traditional internal combustion engine. What makes it different from regular hybrids is its ability to plug in and charge its larger battery from an external power source, like a home charger. This allows the vehicle to drive on electric power alone for shorter trips, helping save fuel and reduce emissions. When the battery runs low or more power is needed, the gasoline engine takes over, extending the driving range. PHEVs offer the best of both worlds: they can run on electricity for daily use while still having the flexibility of a gas engine for longer trips [15].

Power-Split HEV

The power-split hybrid powertrain integrates the strengths of series and parallel hybrid systems using a Power-Split Device (PSD), typically based on a planetary gear set (PGS), to divide engine power into two paths. The mechanical path transmits torque directly to the output shaft through gears, ensuring high efficiency. The electrical path converts torque into electrical energy via one electric motor, which either stores the energy in the battery or sends it to the second motor for propulsion. The planetary gear set consists of three ports (sun gear, ring gear, and carrier), whose

rotational speeds are governed by a fixed mathematical relationship. This allows the engine speed to be decoupled from the vehicle speed, enabling the internal combustion engine to operate consistently in its peak efficiency zone. Additionally, the torques across the three ports of the planetary gear set maintain proportional relationships, necessitating the use of high-torque electric motors to balance the system.This architecture is well-suited for full hybrid vehicles where large electric motors and batteries support high torque demands and efficient energy management. However, it is not suitable for micro or mild hybrid systems due to its reliance on robust electric components and the resulting system complexity [13].

2.1.2 General physical structure of batteries for automotive

A lithium-ion battery pack consists of interrelated subsystems that must work together seamlessly to ensure its functionality, safety, and long-term performance. The integration of these subsystems: cells, mechanical structures, thermal management, Battery Management System (BMS), and electrical components; is crucial. The following subsections will explore each subsystem in detail and discuss how their coordination is essential for the battery pack's reliable operation and meeting its performance targets [14, 16].

Cells

At the core of the pack are the lithium-ion cells. These cells are the primary energy storage units, and their number and arrangement vary depending on the application. Regardless of the specific use case, every battery pack requires a group of cells that are interconnected in various configurations to achieve the desired voltage and energy capacity. The connections can range from simple series or parallel arrangements to more complex combinations [14, 16].

Mechanical Structure

To "hold" and manage these cells, a mechanical structure is implemented. This structure serves multiple purposes: it secures the cells in place, provides physical protection, and often contributes to the thermal management of the system. The mechanical system includes components that connect and align the cells, ensuring they remain stable during operation. Additionally, the structure includes an enclosure that serves as an outer shell, protecting the cells from environmental factors such as moisture, dust, and mechanical impacts. The design of this enclosure is critical not only for safety but also for maintaining the integrity of the cells over the life of the battery [14, 16].

BMS

Within this enclosure is the BMS, an electronic controller responsible for monitoring and managing the operation of the battery pack. The BMS oversees critical parameters such as voltage, current, temperature, and state of charge. By doing so, it prevents conditions that could compromise safety, such as overcharging, overdischarging, or overheating. In some cases, the BMS also incorporates separate electronics installed at the cell or module level. These electronics, often referred to

as voltage temperature monitor (VTM) boards, provide additional localized monitoring of cell voltage and temperature, ensuring the pack operates within its specified limits [14, 16].

Thermal Management System

Another critical subsystem within the battery pack is the thermal management system. This system is essential for regulating the temperature of the cells, as their performance and safety are highly sensitive to temperature variations. Thermal management solutions can range from passive designs, where the enclosure itself acts as a heat sink to dissipate heat naturally, to active systems that force air or liquid through the pack to control its temperature. Active thermal management systems are particularly common in high-performance applications, as they can provide precise temperature control under varying conditions. Some systems also include heating functions, enabling the battery to operate effectively in cold climates [14, 16].

Electrical Components

Lastly, the battery pack includes various electrical components that are fundamental to its functionality. These include switches, contactors, busbars and wiring, which manage the flow of current into and out of the pack. These components ensure the system operates safely and efficiently, controlling when and how energy is delivered or stored [14, 16].

In Figure 2.6 the cost share of a battery pack for HEV is reported from [17]. It highlights that the actual cell part does not represent the highest share in terms of cost in a battery pack. Also for this reason, research is needed to ensure the life reliability of all components in the battery,

2.1.3 Battery components investigated

The following battery components are further investigated based on examples found in literature.

Cells Tab-Tab connections and cell Tab-Busbar connections

In Figure 2.7, a portion of the battery module structure is adapted from [18]. The module consists of multiple cells arranged in a series configuration. One of the cells forming the module is labeled as "n.4" in Figure 2.7. The upper and lower blue structures in the figure represent the heat dissipation pads, which are integral components of the cooling system. These cooling pads play a crucial role in maintaining the pouch cells at a safe and reliable temperature [18].

Figure 2.8 shows a closer view of the cells within the module of Figure 2.7. As illustrated, the cells are electrically connected via cell tabs, conductive strips designed to facilitate electrical connections between the internal components of a battery and external circuits. The tabs are welded together to ensure a secure electrical connection. During operation, factors such as environmental conditions and

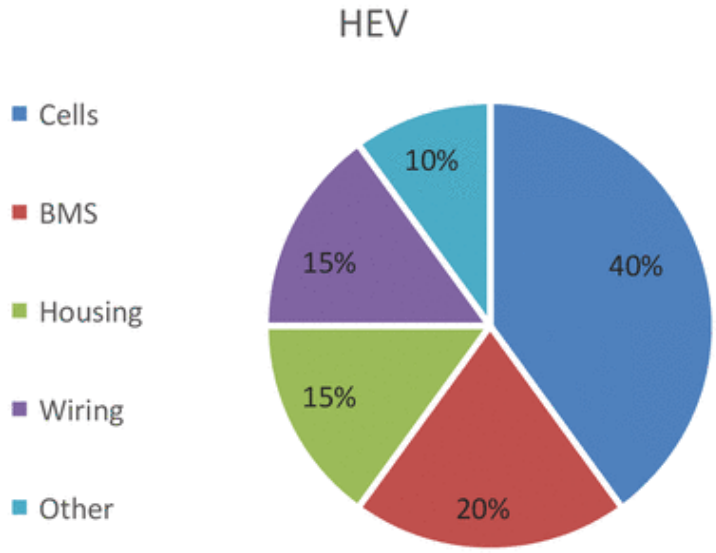

Figure 2.6 Cost share between different components of a HEV battery pack from [17]

current flow cause the tabs to experience heating. This heating effect is primarily due to the intrinsic electrical resistance of both the tabs and their welded joints, as described by the power dissipation formula:

$$P = I^2 R \tag{2.1}$$

In a series configuration, the positive tab of one cell is connected to the negative tab of the adjacent cell. Typically, the positive tab is composed of aluminum, while the negative tab is made of copper. These materials exhibit distinct thermal expansion coefficients. Consequently, temperature fluctuations induce dynamic mechanical stresses at the welded connections due to differential thermal expansion between the two materials. Over time, these stresses make the welded region a critical point of interest for reliability analysis, as it plays a key role in ensuring the long-term performance and efficiency of the battery module. Proper evaluation of this region involves assessing the thermal and mechanical behaviors under various operating conditions, including cyclic loading and extreme temperature variations. Understanding the impact of these factors can aid in designing more robust battery modules with enhanced durability and performance.

Given the aforementioned considerations, the tab welding region has been identified as a critical location for reliability analysis in this Master's thesis work.

Cooling plates fluid collector

Thermal issues substantially impact the performance and longevity of batteries. Therefore, implementing well-designed Battery Thermal Management System (BTMS) is vital to establishing an effective and durable system that can withstand fluctuations in both internal and ambient temperatures. BTMS plays a significant role in improving performance, battery safety, cost-effectiveness, and cycle life. One of the

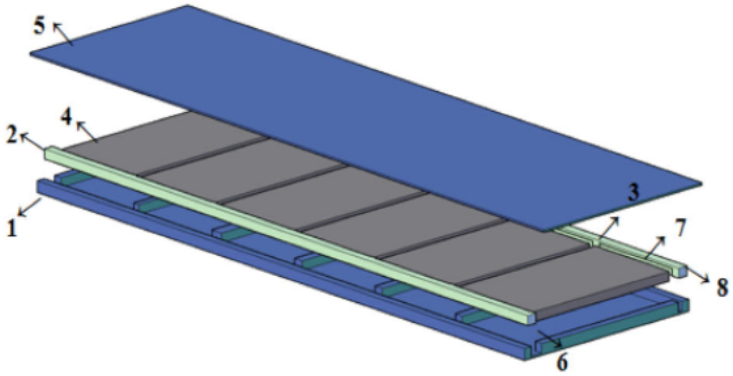

Figure 2.7 [18]

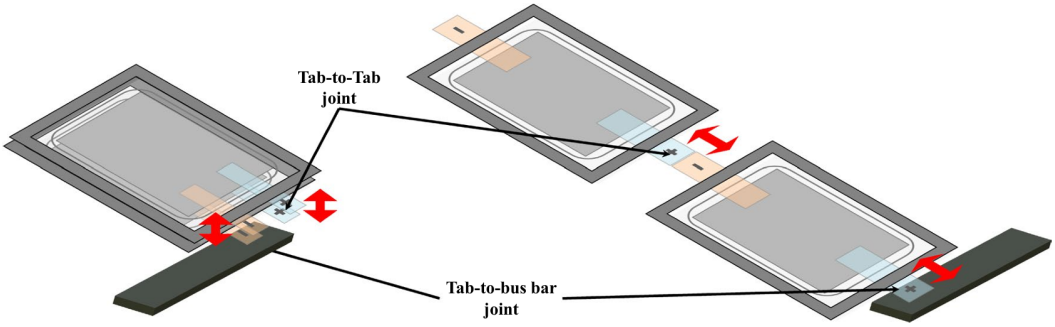

Figure 2.8 [19]

effective methods for thermal management involves the use of heat pipes, which have been employed in several technological applications to improve battery thermal regulation. Heat pipes facilitate both cooling and heating processes, ensuring batteries operate within their optimal temperature range. An established approach in BTMS is the use of refrigerants, where the battery evaporator is connected to the vehicle's air-conditioning evaporator [20]. This configuration results in a compact and efficient system compared to passive air-cooling methods. Another attractive approach is placing the battery evaporator in parallel to the air-conditioning evaporator, offering enhanced thermal efficiency [21]. Tesla Model S and Model 3 used the existing vehicle air-conditioning system to cool the batteries using indirect cooling and cabin air [22]. Refrigerants used in BTMS can be classified into two categories: natural and synthetic. Natural refrigerants include ammonia, carbon dioxide, hydrocarbons, and water. Some of these substances are utilized in boiling-based cooling but are not always considered refrigerants. On the other hand, synthetic refrigerants are divided into four categories: hydrofluorocarbons (HFC), hydrochlorofluorocarbons (HCFC), hydrofluoroolefins (HFO), and hydrofluoroethers (HFE). Each category offers unique properties that contribute to efficient thermal management solutions. A well-designed BTMS is crucial for several reasons, including performance optimization, safety enhancement, longevity improvement, and cost-effectiveness. Proper temperature regulation enhances battery efficiency, ensuring consistent energy output and operational reliability. Overheating

can lead to thermal runaway, which poses safety hazards such as fires and explosions, and effective cooling mitigates these risks. Maintaining an optimal temperature range helps prevent degradation of battery cells, extending their lifespan and reducing replacement costs. By enhancing battery performance and longevity, a robust BTMS reduces maintenance and operational costs over time [20].

Cooling plates and liquid collectors are key components of liquid-based BTMS, which offer efficient heat dissipation compared to air-based systems. Cooling plates facilitate direct heat transfer from battery cells to the cooling medium, such as a liquid coolant, providing uniform temperature distribution and preventing localized hotspots that can degrade battery cells. Liquid collectors efficiently channel the coolant through the cooling circuit, ensuring optimal flow and heat absorption. They connect the internal part of the battery with the external system, with part of the liquid collectors placed outside of the battery where they experience thermal variations and humidity. This external placement makes liquid collectors a critical spot for reliability analysis, as they are exposed to climatic changes in temperature and humidity while also containing coolant with changing temperature inside. In Figure 2.9 a schematic of a general cooling plate is illustrated from [20]. The figure is meant to be the internal part of cooling plate previously illustrated in blue in Figure 2.7 with the addition of the cooling collectors for inflow and outflow of coolant.

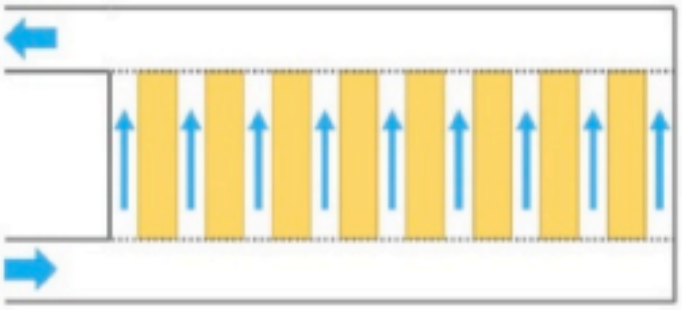

Figure 2.9 Cooling plate and cooling collector general schematics from [20].

2.2 Catastrophic Failure, Thermal runaway

Thermal runaway is widely considered the most serious safety concern in LIBs. Several factors can lead to thermal runaway, such as unwanted side reactions involving the electrolyte, cathode, and anode, as well as interfacial reactions at the electrode surfaces and lithium plating. These reactions are typically triggered by mechanical, thermal, or electrical stress. Accidents, defects, or ineffective control systems can create these stresses, which, in turn, provoke harmful reactions within the battery. Among these, the failure of the separator and the release of oxygen from the cathode are the primary culprits behind thermal runaway. When this happens, it can cause the battery to emit smoke, catch fire, or even explode, with the surrounding air oxygen fueling the fire. Electric vehicle fires are often caused by incidents such as collisions, overcharging, self-ignition, and thermal shocks. These

events can lead to internal short circuits, heat buildup, or localized heat damage, all of which can set off thermal runaway and result in disastrous outcomes

2.2.1 Mechanical abuse

Local damages in LIBs caused by external factors can lead to mechanical failures potentially igniting thermal runaway. Electric Vehicles (EV)'s batteries are subjected to forces while driving that can lead, in extreme cases, in local damage for example like in a car accident [23]. The outer casing of a LIBs serves as the primary shield against both thermal and mechanical stresses. It must be designed to resist mechanical impacts without breaking and protect the internal structure from damage under certain stress conditions. The casing's mechanical performance is vital to the overall safety of the battery, as it is the most likely component to fail during incidents. Therefore, it must be carefully considered when selecting materials for battery design. If the casing is compromised, air can penetrate the battery and react with the internal components, including the electrolytes. Even if the casing is only deformed, parts like current collectors and separators, which lack sufficient flexibility, can crack, causing the electrodes to make direct contact. When the heat from a localized short circuit is substantial, it can set off a chain reaction of internal short circuits, leading to thermal runaway throughout the entire battery [24].

2.2.2 Electrical abuse

Batteries can go through electrical abuse in several ways, such as being overcharged, over-discharged, or exposed to an external short circuit. When this happens, it triggers a series of unwanted reactions inside the battery that can affect its safety and performance. A major cause of overcharging is the inconsistency between the individual cells within the battery. If the battery management system doesn't properly track the voltage of each cell, some cells can end up being overcharged. This is risky because it means the battery is storing more energy than it's designed to handle, which could lead to overheating or internal damage. Normally, batteries are charged to a certain level, known as the State of Charge (SOC). However, sometimes certain cells in the battery might start off with a higher SOC. If those cells are charged any further, they could become overcharged even though the rest of the cells haven't reached their limit yet [25]. This dangerous situation can happen without obvious signs, even if the overall system seems fine [26]. An external short circuit occurs when the cathode and anode of a battery cell come into direct contact with a conductor. This leads to electrons and ions moving simultaneously, causing lithium ions (Li^+) to rapidly migrate inside the cell, discharging the battery quickly. In the event of a safety incident, it is possible for the cathode and anode to touch, resulting in heat being released quickly and evenly across the cell.[6] External short circuits can also occur outside the individual cells, such as within the battery pack itself. A failure in the battery's internal busbars, for instance, can create a short circuit between the positive and negative terminals, or between the positive terminal and ground, and the negative terminal and ground. This type of short circuit can lead to a catastrophic failure, similar to an internal cell short circuit, but occurring externally. The reasons behind the failure are the same: rapid discharge, heat generation, and potential thermal runaway, which can damage the

battery pack and compromise its safety. In addition, any loss of internal insulation within the battery can create a dangerous situation where the battery casing may carry a high electrical potential. This could potentially lead to electrical shocks for users, posing significant safety risks.

2.2.3 Thermal abuse

Thermal abuse in lithium-ion batteries happens when excessive heat, either from external sources or internal heat buildup, creates significant safety concerns [27]. One of the most critical risks is thermal runaway, where the battery's temperature rises uncontrollably, triggering dangerous reactions that can lead to fires or even explosions. Additionally, high temperatures can cause the battery to vent, releasing flammable gases, and can lead to internal short circuits, which worsen the heating and further damage the battery. Over time, prolonged exposure to heat can result in the deformation of the battery's structure [28], leakage of the electrolyte, and a general reduction in battery lifespan. In severe cases, thermal abuse poses risks not only to users, such as the potential for burns or electrical shocks, but also to the environment. Common causes of thermal abuse include overcharging, exposure to high ambient temperatures, and internal faults within the battery. To prevent these issues, effective BMS are essential, as they help monitor and regulate the battery's temperature and overall condition.

2.3 Non Catastrophic Failures

Non-catastrophic failures in LIBs batteries are those that cause a gradual decline in performance rather than sudden, dangerous incidents like fires, explosions, or severe damage. While catastrophic failures can trigger hazards such as thermal runaway or violent reactions, non-catastrophic failures typically occur over time, leading to a slower reduction in the battery's effectiveness and lifespan. Non-catastrophic failures can generally be divided into two categories: loss of functionality and capacity loss. Loss of functionality occurs when a battery can no longer operate as intended, even if its overall capacity remains unaffected. Capacity loss, on the other hand, refers to a gradual decrease in the battery's ability to store and deliver energy.

2.3.1 Loss of functionality

Loss of functionality refers to failures that do not directly reduce battery capacity but impair its operation. These failures do not lead to immediate destruction but can compromise battery performance and reliability over time. One such failure is tab welding degradation, where the electrical connections between cells deteriorate. This can eventually lead to an open circuit, breaking the series connection and rendering the affected portion of the battery inoperative [29, 30]. Another concern is the integrity of the housing welding, which can suffer from mechanical stresses induced by driving vibrations. Over time, micro-cracks may form in the housing structure, expanding gradually and potentially compromising the battery's sealing, exposing internal components to environmental factors and accelerating degradation [31]. Additionally, cooling system connection degradation poses a significant

risk to battery functionality. The cooling system interfaces are exposed to external conditions, including humidity and temperature fluctuations, which can lead to material degradation and connection failure. A compromised cooling system can result in inefficient thermal management, ultimately affecting battery performance and longevity. Another failure mode is enhanced self-discharge, where cells lose charge at an accelerated rate due to internal defects or chemical instability [32]. While self-discharge is a normal phenomenon, excessive self-discharge can cause imbalances between cells, reducing overall efficiency and usability. Furthermore, sensor degradation is a critical issue in battery systems. Sensors monitor key parameters such as voltage, temperature, and current to ensure safe and optimal operation. However, prolonged exposure to environmental stresses like temperature variations, humidity, and vibrations can degrade sensor connections, leading to inaccurate readings or complete signal loss. Such errors can trigger BMS faults, potentially causing the system to shut down, rendering the battery non-functional. Another important failure mode is the increase in resistance of high-voltage busbar connections. During operation, the electrical connections between busbars can degrade over time due to mechanical vibrations, thermal cycling, or material fatigue. This degradation leads to an increase in electrical resistance at the connection points, causing localized heating. The rise in temperature further accelerates degradation, creating a self-reinforcing loop where increased resistance leads to more heat generation, which in turn worsens the connection quality. If not addressed, this thermal instability can significantly impact battery performance, efficiency, and safety [33].

2.3.2 Capacity loss

During the initial charging and discharging cycles of a lithium-ion battery, known as the formation cycles, some of the lithium that would otherwise be available for use is instead consumed to create protective layers on the electrode surfaces. This lithium, often referred to as "cyclable lithium," primarily comes from the lithium stored within the electrode materials themselves. However, a small but meaningful portion, typically less than 15% of the total lithium in the battery, can also come from chemical side reactions involving the lithium salt present in the electrolyte [34]. These side reactions, while essential for stabilizing the electrode surfaces, contribute to the irreversible loss of lithium and are a key factor in the gradual capacity fade of LIBs. Capacity decay during storage and charge-discharge cycling is one of the major challenges that limit the lifespan of LIBs. The instability of the electrolyte at operating potentials leads to side reactions on the electrode surfaces, which result in the formation of Solid Electrolyte Interphase (SEI). This SEI play a crucial role in battery performance but also contribute to lower coulombic efficiency, loss of usable capacity, and an increase in cell impedance. Such degradation, known as chemical degradation, is the primary cause of lithium loss in well-manufactured LIBs. As a result of these reactions, the charge and discharge endpoints gradually shift over time, leading to further performance deterioration. In addition to chemical degradation, the diffusion of lithium atoms in and out of electrode particles induces diffusion-induced stresses (DISs), leading to volume changes in electrode materials during cycling. Depending on operating conditions, these stresses can cause mechanical fatigue, particle fracture, electrode isolation from the composite matrix,

or SEI fracture, further accelerating battery degradation [35]. Mechanical degradation of electrode particles exposes fresh surfaces to the electrolyte, facilitating additional side reactions and contributing to capacity loss. To mitigate the effects of lithium loss and degradation, battery manufacturers often design low-power cells with extra lithium in the positive electrode. This compensates for the initial loss during formation cycles and ensures that the negative electrode's full capacity can still be utilized. However, this approach results in a lower overall energy density compared to an ideal scenario where no lithium loss occurs [34].

2.4 Battery testing steps in design and production

The process of battery design and production in the industry involves multiple interconnected and iterative steps. This pathway is non-linear, beginning with the initial phase focused on the conceptual and technical design of the battery. This phase includes defining performance requirements, selecting suitable materials, and determining the overall configuration. Once the battery design is finalized, a prototype is produced and subjected to rigorous testing to evaluate key performance aspects such as energy density, cycle life, power output, thermal management, and safety features.

During this stage, known as Design Validation (DV), various safety tests are conducted, including short circuit resistance, overcharge and over-discharge protection, and thermal stability tests. Iterative testing and optimization cycles are carried out to identify and address any deficiencies or undesirable behaviors observed in the prototype. The design is refined through these iterations until it meets the required specifications. Once the prototype achieves the desired performance standards, the final design is approved for production.

The next step involves Process Validation (PV), where the manufacturing process is tested and verified to ensure consistent quality in battery production. This phase assesses factors such as material sourcing, assembly processes, and quality control systems to confirm that the production line can reliably produce batteries meeting the required specifications and performance standards. For example, failures due to excessive impurities are typically detected during process validation, thanks to larger-scale testing that includes industrial processes. This stage also involves compliance with regulatory requirements and thorough documentation of procedures, also know as Homologation. Upon successful completion of all these steps, the battery is approved for mass production.

Verification and validation are essential processes to ensure that a product, service, or system adheres to its specifications and fulfills its intended purpose. Broadly speaking, verification assesses whether a product, service, or system meets the defined regulations, specifications, or conditions set at the beginning of a development phase. It acts as a quality control mechanism to confirm that the product is being built correctly according to prescribed guidelines. In contrast, validation ensures that the final product, service, or system performs as intended in real-world conditions and satisfies user needs. Validation is a quality assurance activity designed to demonstrate that the right product has been built to achieve its intended functionality.

While verification focuses on adherence to established standards, validation

prioritizes the effectiveness of the product in meeting practical application requirements. Despite their differences, the terms “verification” and “validation” are often misused or conflated in academic and technical literature. In some cases, they are combined with “testing” under the umbrella of “verification, validation, and testing (VV&T),” with little distinction made between them. This lack of clarity can lead to confusion, as the terminology does not always align with standardized definitions. Various national and international organizations provide precise definitions of verification and validation, often documented in reference materials or summarized in tables to clarify their distinctions and promote consistency across different fields and applications [36, 37]. In Figure 2.10 a schematics of the the majors steps for battery workflow from design to production is reported highliting the non linear process.

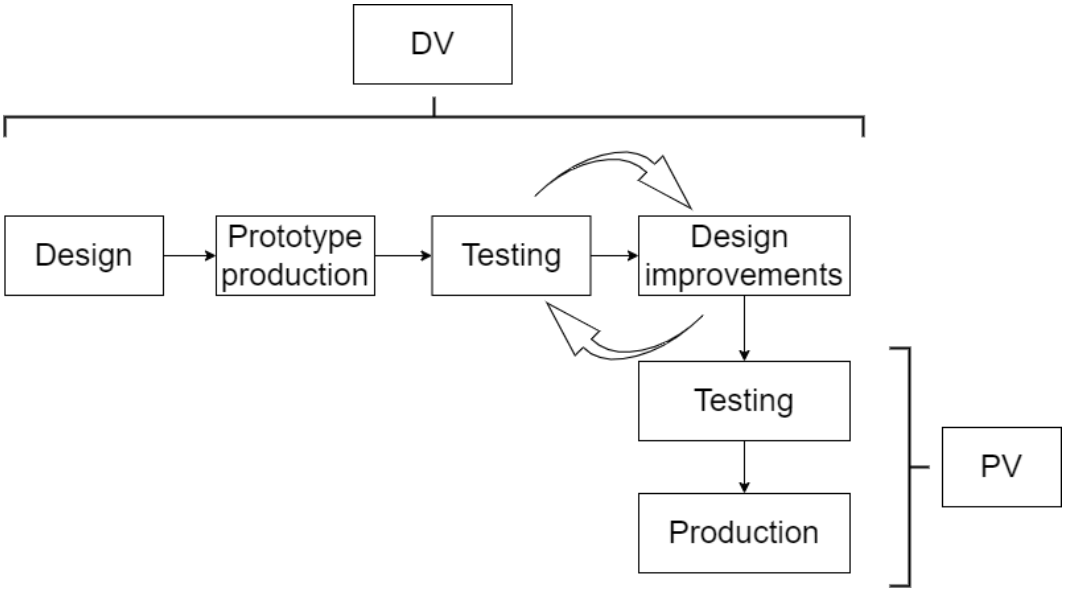

Figure 2.10 Testing steps in battery design and production

2.5 Families of test for battery validation

When it comes to battery validation, there are several distinct families of tests, each aimed at assessing different aspects of a battery’s performance, safety, and longevity. These tests are crucial to ensuring that a battery meets the required standards and functions properly under a range of conditions. Some tests are mandatory for homologation, focusing primarily on confirming the battery’s safety. These tests check for things like thermal stability and electrical safety to ensure the battery can operate without posing risks to users. Homologation tests are often regulatory requirements that must be met to sell or use the battery in specific markets. Beyond these, there is another family of tests known as safety-abuse tests. These tests go further by simulating extreme conditions, such as short circuits, overcharging, or exposure to fire, to see how the battery reacts under worst-case scenarios. While homologation tests ensure the battery meets basic safety standards, safety-abuse tests verify its ability to withstand severe or unexpected conditions. Additionally, characterization tests are designed to confirm that the battery’s performance

matches the expected specifications, evaluating factors such as energy capacity, charging and discharging efficiency, and voltage behavior to ensure it delivers the intended performance. Mechanical tests assess the battery's durability under physical stress, simulating impacts, vibrations, and other mechanical forces it might encounter during transportation, installation, or use. Endurance tests, meanwhile, focus on the long-term durability of the battery, subjecting it to repeated charge and discharge cycles to see how it holds up over time. These tests also evaluate how well the battery performs in harsh environments, like high temperatures, humidity, or rapid temperature changes, ensuring it remains reliable even in challenging conditions. An example of a Venn diagram in Figure 2.11 highlights how some tests overlap across these categories, showing how certain tests can serve multiple purposes, such as assessing both safety and performance. Later chapters will dive deeper into some of these test families and their specific procedures, offering a more detailed understanding of how each test ensures the battery's overall quality and reliability.

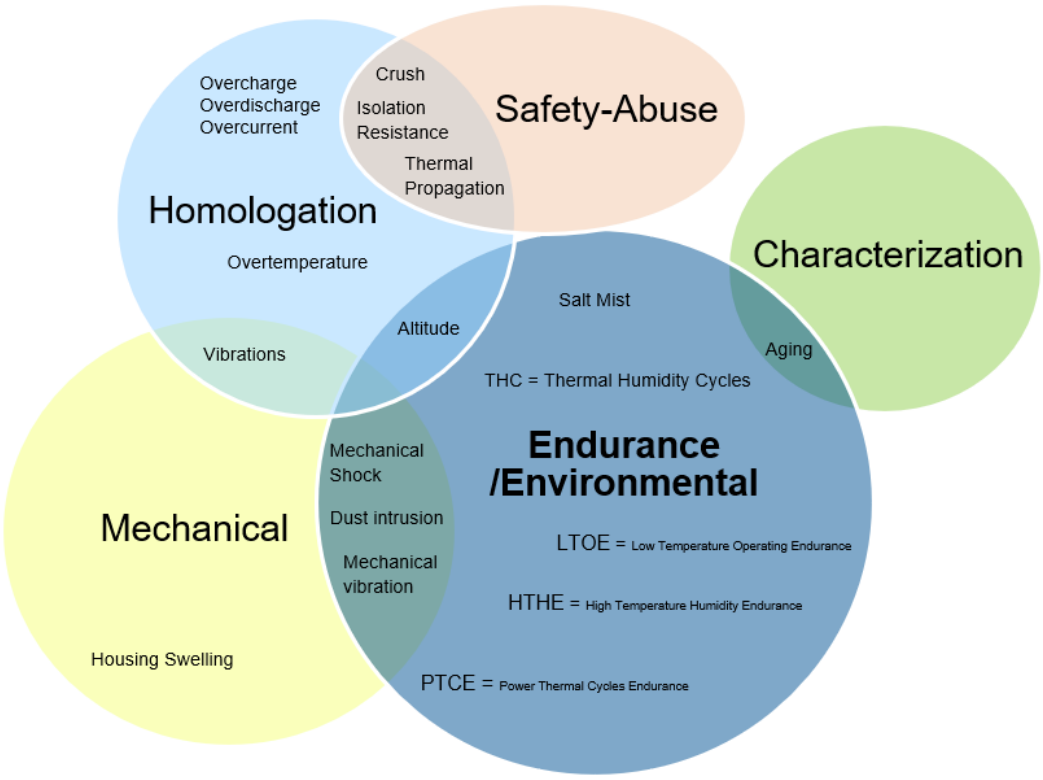

Figure 2.11 Example of a Venn Diagram for battery validation tests

2.5.1 Homologation tests

Homologation tests are a set of standardized procedures used to verify that a product, such as a vehicle or electronic device, meets the required technical and safety standards for its use in a specific region or country. These tests ensure that products comply with the necessary regulations before they are allowed to be sold or used in a given market. The following sections specifically examine the homologa-

tion tests that are required for the transportation of lithium-ion batteries, in accordance with the standards set by the United Nations. [38, 39, 40]

Altitude Test

This test aims to replicate the environmental conditions a battery would face during air transportation, particularly in low-pressure scenarios. To accurately simulate these conditions, both the individual cells and the entire battery assembly must be exposed to a reduced pressure than at sea level for a continuous period of at least six hours. This extended exposure is necessary to evaluate whether the battery can maintain its performance and structural integrity under such conditions, which are typical during transport. The test should be conducted at ambient temperature. The purpose of this test is to ensure that the battery can operate safely and reliably when exposed to the lower atmospheric pressures commonly encountered at high altitudes during air transport.

Thermal Test

This test is intended to assess cell and battery sealing integrity and internal electric connections. The test consists in a rapid and extreme temperature changes. The battery has to be stored for some hours at a temperature of about 70 $^{\circ}C$. Than the battery has to spend same amount of hours at a temperature of -40 $^{\circ}C$ for multiple cycles. After the test the battery has to spend 24 hours at ambient condition. Once the test is done, in order do ensure that the battery is safe and has passed the test, there has to be no leakage, no venting, no disassembly, no rupture and no fire. The Open Circuit Voltage (OCV) drop has to be no more than 10% compared to the test begin. Due to the heat the cell might experience an increase of internal volume due to the gas formation at high temperature. The combination of high temperature and built in pressure could potentially cause cell damages [41].

Vibration Test

The purpose of the test is to simulate the vibration experienced by a battery during transportation. Cells and batteries must be securely fastened to the vibration platform to ensure that the vibrations are accurately transmitted without causing any deformation or damage. The test employs a sinusoidal waveform with a logarithmic frequency sweep that transitions from low to high frequencies and back to low, completed over a specific cycle duration. This cycle is repeated multiple times, resulting in a total test duration of several hours for each of the three mounting positions. One of the vibration directions must be perpendicular to the terminal face.

The frequency sweep starts at low frequencies, maintaining a peak acceleration until mid-test frequencies. After this, the amplitude is held constant, and the frequency increases until the acceleration reaches a higher specified value. From this point onward, the peak acceleration is maintained as the frequency increases to the maximum test frequencies. The test is considered successful if the battery shows no leakage, no mass loss, no venting, no disassembly, no rupture, no fire, and if its OCV drop is less than a specified percentage of the initial value [40, 42].

Mechanical Shock

This procedure is known as a mechanical shock test, which evaluates the durability and reliability of cells and batteries under sudden impact conditions. During the test, the units are securely mounted using a rigid support structure that ensures full contact with all mounting surfaces. The test involves exposing each cell or battery to controlled shock pulses with defined acceleration and duration parameters. The shocks are applied in three mutually perpendicular orientations, with multiple repetitions in both positive and negative directions to simulate real-world mechanical stresses. This comprehensive approach helps assess the structural integrity and performance of the units when subjected to sudden forces. For larger cells and batteries, the testing follows the same principles but with adjusted shock characteristics to accommodate their size and mass. Regardless of size, all units undergo repeated shocks in different orientations to ensure thorough evaluation of their mechanical robustness [40]. To pass the test, the batteries must meet criteria similar to those outlined in the UN38.3 mechanical shock test. These criteria play a key role in homologation processes, ensuring that batteries meet legal requirements for structural integrity. However, it's worth noting that simply meeting these criteria doesn't always guarantee long-term safety or performance. There can be hidden or subtle issues that might go undetected, which could lead to potential failures down the road. For example, [42] presents a case where a cylindrical cell technically passed the test but, when examined using a CT scan, revealed internal deformations that were not initially detected. This underscores the importance of considering additional evaluation methods to gain a more thorough understanding of battery integrity.

This is visible in Figure 2.12.

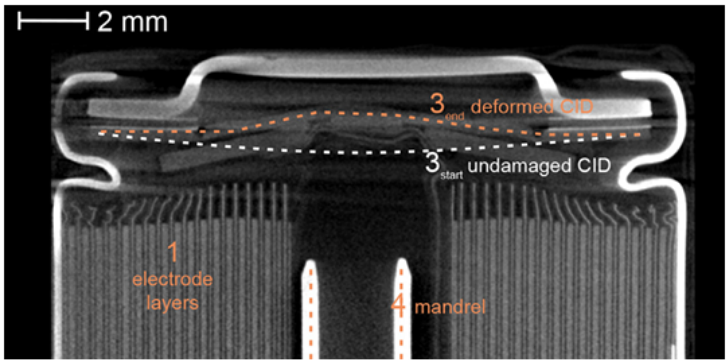

Figure 2.12 Mechanical deformation visible in 18650 cell after 300 shocks in z-direction according to UN38.3 Mechanical shock test [42].

External short circuit

This test is designed to check how safe a cell or battery is under extreme conditions. Before starting the test, the battery is warmed up to a specific temperature and allowed to stabilize. Once it's ready, a short circuit is applied with very low resistance to create a high-current situation, simulating a worst-case scenario. This short-circuit condition is kept in place for a certain period after the battery returns

to its original temperature. After that, it's closely monitored for a few more hours to see how it reacts. To pass the test, the battery must stay within a safe temperature range and must not show any dangerous signs like breaking apart, rupturing, or catching fire.[40].

2.5.2 Safety abuse tests

Abuse tests are extreme, destructive evaluations that simulate worst-case scenarios a battery might face. These include setting the battery on fire, puncturing it with a nail, or crushing it. While these situations wouldn't happen during normal use, they help reveal the battery's safety limits and highlight potential hazards in the most extreme conditions.

Thermal propagation test

In this test, both mechanical and electrical damage is intentionally caused to the battery. A sharp steel rod, called a "nail," is driven through the battery at a constant speed, usually about 8 cm/s [43]. While the result is a short circuit, it's important to note that this short circuit is caused mechanically, which is why this test is considered a mechanical test rather than an electrical one. As the nail punctures the cell, it disrupts the separator and electrodes, creating short circuits and generating heat. Since several electrode layers are in contact with each other, and the short circuit happens at the point of penetration, the damage occurs quickly. Additionally, because the damage is localized to a small area, heat can't escape easily, causing the temperature to rise rapidly. [44]. The scope of the test is to ensure that the thermal event does not propagate to other cells rather than the one damaged.

2.5.3 Battery characterization tests

Testing a battery's performance is key to ensuring that it can meet the specific needs of its intended application, such as in an electric vehicle. To do this, a series of tests are performed where the battery is charged and discharged under controlled conditions, using predefined current or power levels. These tests are designed to check whether the battery's performance matches what's expected. The results are compared with standard values for important parameters, like capacity (measured in ampere-hours [Ah]), energy (measured in watt-hours [Wh]), maximum current (in amperes [A]), and power (in watts [W]) [45]. For example, it's important to verify that the battery's capacity is in line with expectations because this directly affects how much energy the battery can store and provide. In electric vehicles, the battery must be able to deliver enough power to ensure the car can travel the required distance. So, it's essential that the battery's performance matches the design goals to make sure the vehicle performs as planned. In the following sub-chapters the most common tests are reported.

Constant Current discharge and static capacity

In this test, the battery is first fully charged and then simply fully discharged with a constant current until a limiting cutoff voltage specified by the battery manufacturer is reached. The constant discharging current is based on the Nominal capacity

(C) of the cell and its intended application. The C rate is the current in amperes corresponding to the 1-h capacity in ampere-hours. As an example, if a battery has a nominal capacity of 20Ah, then the current corresponding to 1 C rate is 20A and the battery gets fully discharged in 1 hour, the current corresponding to 2C rate is 40A, and with this current, the battery is fully discharged in 30 minutes. If the battery is designed for high power and low energy density, the test C rate could be of 1C or even 10C according to standards like IEC 62660-1, and ISO 12405-1 [45]. This test is done to check if the measured capacity in ampere hours and the corresponding energy content in watt-hours agree with the values provided by the manufacturer. It is also repeated after cycling to check for capacity loss [46, 45]. In figure 2.13, the result of a capacity test at the beginning of the life of a Lithium Iron Phosphate battery (LFP) battery compared to the same test carried out at different cycle numbers is reported from [47]. Figure 2.13 is intended to be read

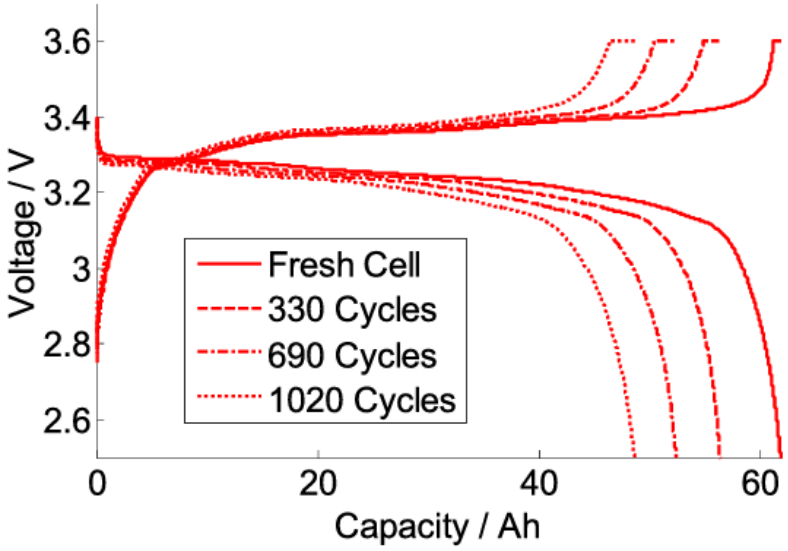

Figure 2.13 Capacity [Ah] Vs. Voltage [V] of an LFP battery rated 60 Ah from [47].

from bottom left to top right for charging situations and from top left to bottom right for discharging situations. As can be seen, during fresh cell charging, a maximum voltage of 3.6 volts is reached together with a capacity of 60 ampere-hours. After 1020 cycles, the maximum voltage stays similar, but the capacity gets reduced due to aging [47].

Pulse power characterization and internal resistance

The pulse power characterization test focuses on evaluating the battery's dynamic behavior when exposed to rapid current pulses. In this test, the battery undergoes a high current discharge pulse, simulating acceleration, immediately followed by a high current charge pulse, representing regenerative braking. This setup mimics the transient current demands that electric vehicle (EV) batteries experience in real-world conditions. The primary goal is to assess how the battery responds to these quick fluctuations in current, particularly its ability to handle sudden voltage drops during discharge and surges during charging. This provides valuable insights into

the battery's power performance and internal resistance under dynamic operating conditions. Pulse tests are essential for evaluating how batteries perform under dynamic load conditions. During discharge, the pulse typically uses the full normalized current (100%), while charge pulses usually operate at a reduced level, such as 75%, to account for the partial energy recovery observed in simulated braking scenarios. The duration of these pulses depends on the specific application. For high-power applications, as specified in ISO 12405-1, the pulse lasts between 0.1 s and 20 s. In contrast, high-energy applications, outlined in ISO 12405-2, can have pulses extending up to 120 s. Generally, charge pulses are shorter than discharge pulses, but the exact magnitude and duration can vary based on testing requirements. One of the main objectives of pulse testing is to determine the battery's internal resistance (R). This is done by analyzing the relationship between the change in voltage (ΔV) and the change in current (ΔI). The ohmic resistance is calculated using the following formula:

$$R = \frac{\Delta V}{\Delta I} \tag{2.2}$$

Both charge and discharge pulses are examined to assess the battery's response to sudden load variations. This provides critical insights into its electrical behavior and performance under real-world operating conditions. [47].

2.5.4 Endurance and environmental tests

Power Thermal Cycle Endurance (PTCE)

The PTCE test is an accelerated evaluation method that mimics the thermal and thermomechanical stresses a component experiences during a vehicle's service life. The purpose of the test is to assess the component's quality and reliability by identifying potential failures caused by temperature variations and associated mechanical strain [48]. In everyday vehicle use, temperatures constantly fluctuate, creating mechanical stress on nearby materials. This stress can lead to failures such as cracked solder joints, damaged circuit boards, broken seals, or disrupted traces. The PTCE test is designed to replicate these conditions, focusing specifically on solder joint failures, which are a common issue in electrical and electronic components [41]. The test must either directly correspond to the thermomechanical conditions expected over the component's lifespan or maintain a proportional relationship to those conditions. Without this alignment, it would be impossible to gauge the sample's reliability or confidently determine if the product might fail during actual use [49]. Figure 2.14 reports the temperature oscillation in the PTCE profile and it could be also applicable for the Temperature Cycling test present in ISO 16750-4 standard [50, 41]. In Figure 2.14 can be seen that the test is designed with a temperature changing from Tenv.max or Top.max to Tenv.min or Top.min. These temperatures represent the maximum and minimum temperatures the component would experience in its life. The single 2.14 cycle can be repeated multiple times to increase the component's testing stresses to match the total stress seen in component's life thanks to Coffin-Manson model introduced later on. The temperature ramp rate should be between 4 $^{\circ}C/Min$ to 10 $^{\circ}C/Min$. The tested component should be tested in a non operating or low power mode [41].

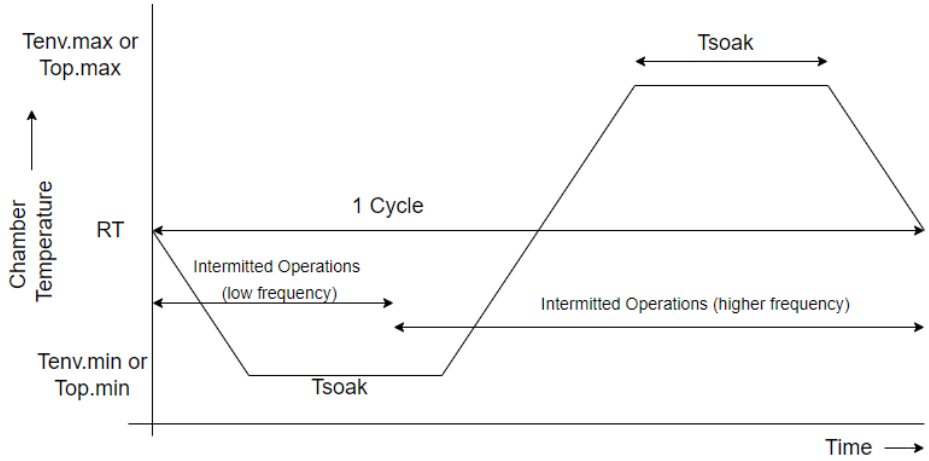

Figure 2.14 PTCE single cycle profile with only one extreme temperature.

High Temperature & High Humidity Cycle Test (HTHE)

The HTHE also known as Damp heat cyclic test, simulates the impact of high temperatures and high humidity on the battery's functionality and safety over extended periods of time [41], it is often used to simulate tropical or highly humid environments [51]. HTHE test is meant to stress the component with respect to failures that can occur in several ways, including electrical shorts caused by oxidation or galvanic corrosion of metals. Oxidation happens when metals react with moisture and oxygen, forming a layer that interferes with electrical conductivity. Galvanic corrosion, on the other hand, happens when two different metals come into contact with moisture, causing one metal to corrode while the other remains unaffected. This can lead to the deterioration of connectors and circuit boards, resulting in electrical malfunctions [52]. In addition to electrical issues, materials can absorb water, which can lead to swelling and a loss of strength. This can disrupt the performance of components and cause adhesives, potting compounds, sealants, and conformal coatings to fail. When these materials absorb moisture, they lose their ability to bond, insulate, or protect, weakening the overall structure of the component. These moisture-induced failures are particularly concerning in electronic devices, automotive parts, and other components exposed to humid or wet environments. Over time, this can result in reduced performance and potential failure of the device. The test temperature should be high, around $90°C$, and the relative humidity should be around 85%.

Thermal Humidity Cycle (THC)

Moisture buildup, either from everyday driving conditions or frost formation in cold climates, can lead to component or device failures over time. This testing process ensures that components remain reliable when exposed to moisture fluctuations. If water becomes trapped in small internal spaces, it can freeze and expand, potentially causing mechanical damage [41]. It is important to understand how environmental factors like temperature and humidity affect the performance and longevity of the battery. For example during day/night temperature cycling, the battery is exposed to fluctuating temperatures, causing expansion and contraction of internal

components. This stress can lead to reduced performance and potential degradation over time. Similarly, humidity cycling exposes the battery to varying humidity levels, which can lead to internal short circuits, corrosion, or electrolyte degradation. If the battery is housed in a case with small holes, the interaction between the internal and external environment is heightened. These holes allow moisture to enter more easily, which could cause condensation, corrosion, or leakage inside the case. The battery's housing design is crucial in protecting it from humidity and temperature extremes. Therefore, testing should assess not only the battery's performance under temperature and humidity conditions but also how well the housing prevents moisture infiltration and maintains its integrity [51]. When air cools down at a specific relative humidity, it can eventually reach a temperature known as the dew point. At this temperature, the air becomes fully saturated with moisture (relative humidity reaches 100%) and can no longer hold all the water vapor. Any further cooling causes the excess moisture to condense into liquid, forming dew, fog, or condensation on surfaces. On a psychrometric chart, this process is easy to visualize. As the temperature drops, the air's state moves horizontally to the left, closer to the saturation curve. Once it touches this curve, the air has reached the dew point. For example, if the air starts at 50% relative humidity, cooling it without changing the amount of water vapor will eventually bring it to the dew point, where condensation begins. The HTHE could also be called a dew condensation cycle test because a rapid change in temperature can lead to condensation due to the high humidity. In Figure 2.15, a psychrometric chart is provided to illustrate this concept.

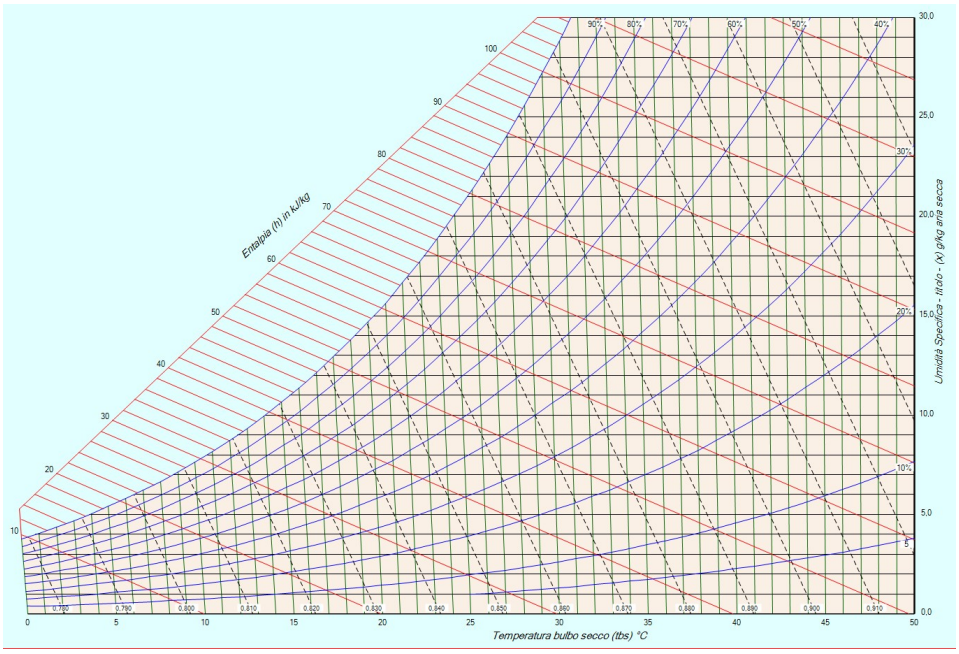

Figure 2.15 Psychrometric chart.

The testing temperature oscillates from -10 $^{\circ}C$ to +65 $^{\circ}C$ to include the effect of freezing conditions on components. When temperature is high, the relative humidity during the test should be 95% in order to force condensation and freezing during cold phase.

High Temperature Operating Endurance Cycle (HTOE)

The HTOE test is conduced at maximum possible operating temperature. The test object should be powered and operating to mimic real life. This process depends on both time and temperature, aiming to test components by exposing them to sustained high temperatures while they are actively functioning. The purpose is to accelerate and reveal failure mechanisms that are driven by heat and diffusion [53].

Chapter 3

Physics of failure reliability assessment

The PoF approach is a method used in reliability engineering to predict how long a product will last under real-world conditions. Unlike traditional methods that rely on past failure data, PoF focuses on understanding the physical, chemical, and mechanical processes that cause a product to degrade over time. By studying these degradation mechanisms, engineers can identify potential failure points and create models to estimate the product's lifespan. This approach not only improves the accuracy of reliability predictions but also helps in designing better, more durable products [54].

Reliability is defined as the ability of a product or system to perform its intended function for a specified time under its expected operating conditions [55]. To ensure product reliability it is essential to understand how the product will be used and for what length of time. This topic is further explained later on in the sub chapter 4.2.

Time to Failure (TTF) is a concept used in reliability engineering, defined as the duration from the beginning of the operation or use of a system or component until it experiences a failure that prevents it from performing its intended function. PoF reliability estimation uses physics-based models to estimate the TTF for the product investigated. The physics-based models used identify the specific mechanisms that lead to device failure and measure the TTF by thoroughly understanding the materials involved and the stress conditions the device will face [56]. Here a fundamental distinction between Failure Modes and Failure Mechanisms is reported. **Failure Mode** refers to the actual observation of failure. For example a welding joint disconnection in a battery's busbar is a failure mode. The underlying process that causes the failure is defined instead as **Failure Mechanism**. A failure mechanism may involve physical, chemical, thermodynamic, or various other processes that lead to a failure. Being consistent with the previous busbar example, the failure mechanism leading to this failure mode could be the fatigue due to non homogeneous thermal expansion of the welded materials when temperature increases due to the ohmic resistance during power delivery.

3.1 Needs to short testing time maintaining testing significance

In today's fast-paced and competitive global economy, engineers are often under pressure to evaluate the reliability of products within a limited time-frame. This challenge is especially significant for devices designed to last 10 years or more. It is neither practical nor cost-effective for a company to spend a decade testing a device to determine its reliability over its entire expected lifespan. Instead, engineers must rely on accelerated testing techniques and predictive modeling to estimate long-term reliability in a much shorter period. These methods enable the identification of potential failure mechanisms and allow for the assessment of a device's performance under conditions that simulate extended use. By leveraging these advanced techniques, companies can ensure their products meet reliability standards and remain competitive in the market, without incurring the excessive time and costs associated with prolonged testing. Accelerated test can be based on time compression or stress elevation. [54]. Time compression accelerated tests are based on the concept of maintaining stress levels within operational limits while increasing the frequency of operations to simulate the total number of cycles expected over the device's lifetime. This approach allows engineers to predict long-term reliability without exceeding the normal stress conditions that the device would encounter during regular use. Stress elevation accelerated tests are based on the concept of increasing one or more load levels, such as temperature or voltage, beyond those expected during normal operation. By operating under these elevated stress conditions, failures are induced in a shorter time frame, allowing for quicker assessment of the device's reliability. In the battery field, the extra challenge in stress elevation tests also comes from safety limitations in enhancing loads such as temperature or operational current. The successful implementation of a stress elevation accelerated test is strongly related to the implementation of an acceleration model, translating the time spent under test conditions to the equivalent time in real-world operational environments. A test can only be classified as an accelerated life testing (ALT) when an appropriate acceleration model is established. This model is essential for interpreting the accelerated test data and correlating it with the expected performance and lifespan of the device under normal operating conditions. Without a well-defined acceleration model, the test results cannot be accurately extrapolated to predict real-world reliability.

3.2 Introduction of equivalent fatigue models in literature (compare Accelerated test damage to Cycle damage)

As briefly mentioned in sub chapter 3.1, establishing an acceleration model for each failure mode and test is essential to correlate the time under test to the time in the field. Making sure that the acceleration model is valid enables to prove that the cumulative damages the component will accumulate during its operating life will be equivalent to the damages accumulated during the accelerated test. In the following sub chapters the investigated acceleration models are reportend and analysed

3.2.1 Coffin-Manson Model

The Coffin-Mason Model is a widely used empirical model to describe fatigue life of materials under shear strain due to thermal cycling. It is particularly useful to identify the cycles to failure of welded joints composed of different thermal expansion coefficient materials.

$$N_f = A \left[\frac{1}{(\text{Shear\_Strain})^2} \right] \tag{3.1}$$

Where N_f is the number of shear cycles to failure and A is an empirical constant.

In this context, we explore the non-linear relationship between shear strain and damage in electronic components. The exponent value of 2 in the strain-damage equation indicates that damage increases non-linearly with strain. Consequently, numerous low-level shear events can be considered negligible, while the focus should be on understanding the impact of fewer, high-magnitude shear events. [57].

When materials with different coefficients of thermal expansion undergo temperature changes, the resulting shear strain is directly proportional to the temperature change (ΔT). Larger temperature fluctuations (ΔT) are more critical than smaller ones, as they have a more significant impact on the integrity of electronic components. This principle can be generalized to emphasize the importance of high-magnitude thermal events over minor temperature variations. The previous equation can be manipulated introducing the temperature variation and the number of cycles to failure can be computed as:

$$N_f = \frac{A}{(\Delta T)^C} \tag{3.2}$$

Where the exponent C is approximately 2 for soldered joints materials.[58]. Considering N_f the number of cycles to failure expected during life in operation and N_a the number of cycles to failure during accelerated test, the equation can be rewritten expressing the acceleration factor AF:

$$AF = \frac{N_a}{N_f} = \left(\frac{\Delta T_f}{\Delta T_a} \right)^C \tag{3.3}$$

This equation can be applied to design accelerated thermal cycling tests that generate shear fatigue damage in solder joints equivalent to real-world conditions. If AF = 1 the accelerated thermal test generates the same damage expected during life IF AF > 1 the accelerated thermal test generates an higher damage than expected during life. [59]. In figure 3.1 the Acceleration Factor Vs. $\frac{\Delta T_f}{\Delta T_a}$ is reported with five different C constants ranging from 1 to 3.

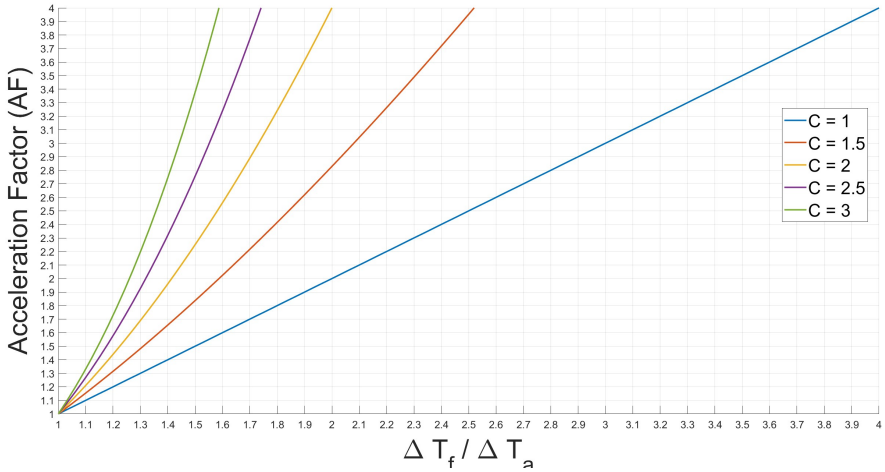

Figure 3.1 Acceleration Factor Vs. $\frac{\Delta T_f}{\Delta T_a}$

Equivalent shear stress PTCE example

In this section the Coffin-Manson model is used to give a computational example to estimate the accelerated test (PTCE) cycle number (N_a) for equivalent shear stress in welded joints. Lets assume a welded joint in the battery pack is in life subjected to an average typical ΔT_f of 34 °C for a number of N_f of 8200 cycles during life. In operation however the component can reach extreme temperatures from -40 °C up to +85 °C. A ΔT_a of 125 °C can be set for accelerated test temperature. Rearranging equation 3.3, N_a can be computed:

$$N_a = N_f \left(\frac{\Delta T_f}{\Delta T_a} \right)^C \tag{3.4}$$

Inserting the given values into equation 3.4 and considering C=2 [59] for welded joints, the equation becomes:

$$N_a = 8200\,\textit{cycles} * \left(\frac{34}{125} \right)^2 = 607\,\textit{cycles} \tag{3.5}$$

3.2.2 Arrhenius Model

The Arrhenius model, originally developed as a phenomenological equation to describe the temperature dependence of chemical reaction rates, has become a foundational tool for analyzing temperature-induced processes and degradation phenomena across a wide range of disciplines. The model is mathematically expressed as:

$$K = C \exp\left(-\frac{E_a}{RT} \right) \tag{3.6}$$

where K represents the rate constant of the process, C is the pre-exponential factor reflecting the frequency of successful molecular collisions, E_a is the activation energy that defines the energy barrier for the reaction, R is the universal gas constant also known as Boltzmann constant = 8.617 x 10-5 eV/K), and T is the absolute

temperature in kelvin [59]. By demonstrating an exponential relationship between reaction rates and temperature, the Arrhenius model has been extended beyond its original chemical context to include the study of temperature-driven processes in materials science, electronic components, and electrochemical systems, such as lithium-ion and zinc-based batteries [60]. In the context of battery reliability and life prediction, the Arrhenius equation has proven particularly useful for modeling degradation mechanisms, such as SEI layer growth, lithium plating, and particle cracking, all of which are strongly temperature-dependent. Moreover, the model is often used in conjunction with the Q_{10} factor, a metric that quantifies how the rate of a process changes with a 10 ℃ increase in temperature. For instance, studies on zinc-based batteries have employed the Arrhenius model to predict their lifespan under varying temperature conditions, while research on lithium-ion batteries has highlighted its effectiveness in analyzing accelerated degradation due to elevated storage and cycling temperatures [60]. When plotted on a logarithmic scale, the Arrhenius equation produces a linear relationship between the natural logarithm of the rate constant ($\ln K$) and the inverse of the absolute temperature ($1/T$), allowing for straightforward estimation of activation energy from experimental data. This characteristic makes it an invaluable tool in the design of accelerated testing methodologies, enabling the identification of critical thresholds for thermal stability and degradation. However, its application must be carefully calibrated to avoid over-simplifications, as degradation in complex systems often involves multiple interacting mechanisms, each with distinct activation energies and dependencies on temperature. Consequently, combining the Arrhenius model with experimental validation across different operational conditions ensures more accurate and reliable predictions of system performance and failure. The continued application of the Arrhenius model in the reliability testing of batteries, as demonstrated in studies of zinc-based and lithium-ion technologies, underscores its versatility and importance. By providing insights into temperature-sensitive failure mechanisms and facilitating the development of predictive frameworks, the model remains an essential tool for optimizing the design, operation, and longevity of energy storage systems [61].

The E_a is expressed in electron volt [eV] and it is different for each Failure Mechanism. The higher the E_a, the higher is the degradation process. In Table 3.1 different activation energies are reported from [59]:

Table 3.1 Failure Mechanism and Activation Energy Constant [eV]

Failure Mechanism	E_a **[eV]**
Dielectric breakdown	0.3 to 0.6
Diffusion failures	0.5
Corrosion - electrolysis	0.3 to 0.6
Corrosion - chemical and galvanic	0.6 to 0.7
Electro-migration	0.5 to 1.2
Charge loss (MOS/EPROM)	0.8
Ionic contamination	1.0
Surface charge accumulation in silicon oxide	1.0 to 1.05
Aluminum penetration into silicon	1.4 to 1.6

The Arrhenius model is widely used to estimate the lifetime of electronic components operating at constant temperatures, where failure mechanisms are governed

by molecular processes. The Acceleration Factor (AF) quantifies the relationship between the usage time under normal field conditions and the equivalent time under accelerated test conditions. By incorporating the Arrhenius equation, the acceleration factor can be expressed as:

$$AF = e^{\frac{-E_a}{R}\left[\frac{1}{T_a}-\frac{1}{T_s}\right]}, \tag{3.7}$$

With T_a = Accelerated test temperature in °K and T_s = Field service temperature in °K.

The total testing time is given in equation 3.8 where p_i and $A_{T,i}$ are the portion of time the component is subjected to a specific climatic regime and the corresponding acceleration factor.

$$t_{\text{test}} = t_{\text{operation}} \sum_i \frac{p_i}{A_{T,i}} \tag{3.8}$$

3.2.3 Lawson Model

The Lawson Model is used to understand how temperature and humidity influence the failure lifespan of electronic components. This model is commonly applied to accelerate the High Temperature and High Humidity Cycle Test. It incorporates the combined effects of elevated temperature and relative humidity into a mathematical model, expressed through equations 3.9 and 3.10, which calculates the acceleration factors [62].

The part of the model describing the temperature dependency is the following:

$$AF_T = e^{\left[-\frac{E_a}{R}\left(\frac{1}{T_a}-\frac{1}{T_f}\right)\right]} \tag{3.9}$$

Where:

- AF_T = The temperature acceleration factor.
- E_A = Activation energy [eV].
- R = Boltzmann constant ($k = 8.617 \times 10^{-5}$ eV/°K).
- T_a = The temperature of the accelerated test.
- T_f = The field temperature condition.
- T = Absolute Kelvin temperature (°K).

It is important to remark that equation 3.9 looks similar to the Arrhenius model but the activation energy E_A differs between them because the two models describe completely different failure modes.

The part of the model describing the humidity dependency is the following

$$AF_{RH} = e^{b\left[RH_a^2 - RH_f^2\right]} \tag{3.10}$$

Where:

- AF_{RH} = The relative humidity acceleration factor.

- b = non dimensional constant.
- RH = Relative Humidity measurement as %.
- RH_a = Relative humidity during accelerated tests.
- RH_f = Humidity during operation.

The total Lawson model acceleration factor is the combination of AF_T and AF_{RH} expressed in the following equation:

$$AF_{T,RH} = e^{\left[-\frac{E_a}{R}\left(\frac{1}{T_a}-\frac{1}{T_f}\right)\right]+b\left[RH_a^2-RH_f^2\right]} \tag{3.11}$$

[59].

The Lawson Model is used in this work to model the damage accumulated at the cooling plates fluid collector illustrated in sub-chapter 2.1.3.

Equivalent HTHE test duration example

Let's assume a component is mounted on a vehicle. The average temperature during non-operating time is 23 Celsius and the relative humidity is 65% if the test conditions are 85 Celsius and 85% relative humidity, the test acceleration factor is 129.3.

Chapter 4

Endurance tests dimensioning

4.1 Vehicle's life target expectation

To accurately assess the reliability of a product, it is essential to first establish the intended lifespan of the product. This lifespan depends on several factors, including the type of product, the specific market segment it is designed for, customer expectations, and the brand values upheld by the manufacturer. Engineering judgment, combined with economic considerations, plays a crucial role in defining the boundary conditions for the product's operational life. In the automotive industry, each manufacturer typically sets its own life targets for vehicle components. These life targets are determined based on the expected duration or mileage that a component should function properly without significant failures. The expectations are generally based on statistical analysis of customer usage patterns to ensure the components meet performance and reliability requirements.

A practical example of life target determination can be observed in Volkswagen AG, where component reliability targets are set based on customer usage statistics. Specifically, Volkswagen AG defines the lifespan of vehicle components based on on expected service life of 15 years and an expected mileage of 300000 km [41]. This approach ensures that components remain reliable under typical operating conditions and minimizes the likelihood of premature failures. Once the overall vehicle life target is determined, it must be further contextualized into specific requirements for individual components. These component-specific requirements define durability targets in terms of operating conditions and expected stress cycles. For example, considering the expected vehicle life and an assumed number of trips per day, the number of engine on/off cycles that a vehicle's engine must withstand over its operational life can be estimated. For heavy-duty diesel engines or other applications where a longer lifespan is expected, these life targets may be adjusted to ensure that the product meets the durability expectations required for extended use.

In the case of vehicles that are either partially or fully powered by electric motors, the battery life target should be aligned with the expected lifespan of the vehicle itself. This is crucial because the battery is one of the most critical and expensive components in an electric vehicle. Automotive lithium-ion batteries are generally considered to have reached their End of Life (EOL) when their capacity degrades to 80% of their initial value [63]. This capacity fade indicates a signifi-

cant reduction in the battery's ability to store and deliver energy, thereby impacting vehicle performance and range. Battery aging is a complex process that can be categorized into two main types: calendar aging and cycle aging. Calendar aging refers to the gradual degradation of the battery over time, even when it is not actively in use. Factors contributing to calendar aging include temperature exposure, state of charge (SOC) during storage, and the duration for which the battery remains idle. Cycle aging, on the other hand, occurs due to repeated charge and discharge cycles. It is influenced by a range of factors, including temperature, SOC, variations in SOC (ΔSOC), the magnitude of charging and discharging currents, charging and discharging cut-off voltages, and the applied charging protocols [63].

From the discussion of battery loss of functionality in sub-chapter 2.3.1, calendar and cycle aging, it is evident that battery longevity is strongly influenced by how the vehicle is used. The driving cycles that each customer follows, along with their driving styles and habits, play a significant role in determining how quickly a battery degrades. Frequent rapid accelerations, aggressive braking, and prolonged high-speed driving can contribute to faster degradation, while conservative driving and optimal charging practices can extend battery life. Understanding these aging mechanisms is essential for designing effective battery management systems that optimize performance and prolong battery lifespan, ensuring that the battery remains functional and reliable throughout the vehicle's operational life.

4.2 Reference driving cycles for customer usage & Life Mission definition.

To accurately assess the stresses that the car's battery will endure throughout its operational lifetime, it is essential to first establish the expected usage profile of the vehicle. This study is conducted in collaboration with a well-known racing car manufacturer based in Modena, Italy. Given the company's specialization in luxury racing cars, its customer base is highly targeted and well-defined, consisting of individuals who seek high-performance vehicles for both regular driving and track experiences.

Based on statistical analyses and engineering judgment, it is assumed that the vehicle will remain parked for extended periods compared to a conventional economy car, which is typically used more frequently for daily commuting. In defining the conditions under which the car is expected to remain parked, two primary scenarios have been established to account for both an average usage profile and a highly aging profile. The standard customer is expected to park the vehicle at a moderate ambient temperature of 20 ℃ and a relative humidity of 65%, leading to relatively slow battery aging and slow loss of functionality issue development. Conversely, the most severe customer usage scenario involves parking the car at 40 ℃ and a relative humidity of 90% , resulting in significantly accelerated calendar aging and an faster development of loss of functionality issues as stated in sub-chapter 2.3.1.

In terms of active usage, the car is primarily driven on weekends, typically covering short driving distances. Given the nature of the manufacturer and its racing heritage, it is reasonable to expect that a significant proportion of owners will operate their vehicles at maximum performance levels on dedicated race tracks to fully exploit the car's capabilities.

Aside from high-performance track usage, the average customer is also expected to drive the car over shorter distances on highways, including those without speed restrictions, such as certain sections of the German Autobahn. Since this thesis focuses on a plug-in hybrid electric vehicle (PHEV), it is important to highlight that a full-electric operating mode is possible for limited distances. When considering the vehicle's charging conditions, it has been established that at-home charging will typically occur at a power rate of C/2.

Another important aspect of the vehicle's operational environment is exposure to high-vibration road conditions. During its lifetime, the car is expected to travel over uneven surfaces that generate significant vibrational stresses, such as Modenese cobblestone streets. While the vehicle's suspension system is designed to filter out a portion of these vibrations, some level of mechanical stress will inevitably be transferred to the battery pack, potentially affecting its performance and longevity.

To systematically assess the complete range of conditions to which the car will be exposed, a concept known as the "Life Mission" is introduced. A Life Mission is defined as the combination of all possible driving, parking, and charging conditions (referred to as profiles) that the vehicle will experience. Each profile is assigned a corresponding repetition factor, indicating the number of times the vehicle will be subjected to a specific condition throughout its lifetime. Establishing a Life Mission is a crucial step in identifying all relevant stress factors affecting the vehicle's battery system and serves as a foundation for designing validation tests that appropriately replicate real-world conditions.

Table 4.1 provides a structured overview of the driving profiles included in the Life Mission, along with the mathematical formula used to compute the total driving mission. Similarly, Table 4.2 outlines the assumed conditions under which the car will be parked when not in active use.

Profile list	L_i **Profile length [km]**	R_i **Profile repetitions**
Profile 1	a	x
Profile 2	b	y
Profile 3	c	z
Profile n	...	...
Profile $n+1$	...	...
Driving Life Mission [km]		$\sum_{i=1}^{n+1}(L_i \cdot R_i)$

Table 4.1 Driving Profiles Table with Driving Life Mission Calculation

	Temperature [C]	**Relative Humidity [%]**
Parking Mode 1	20	65
Parking Mode 2	40	90

Table 4.2 Parking Mode Conditions

By clearly defining the Life Mission and associated operational conditions, it becomes possible to develop a structured approach to battery validation testing. This approach ensures that the imposed stress conditions adequately replicate real-world scenarios, facilitating a more accurate evaluation of battery performance,

degradation mechanisms, and overall longevity under typical customer usage conditions.

4.3 Simulated battery response to customer driving cycles

Once the different driving, parking, and charging conditions throughout the vehicle's lifespan have been defined, simulations are conducted to predict the battery behavior under operational conditions. These simulations incorporate a wide range of driving and environmental parameters to replicate real-world scenarios as accurately as possible. The inputs include vehicle speed profiles, ambient temperature variations, load demands, and energy management strategies. By considering these diverse factors, the simulations provide a comprehensive understanding of battery performance over time.

As a result of these simulations, multiple data types are generated, offering insights into the battery's operational characteristics. Among the key outputs are the state of charge (SOC), input and output currents, voltage fluctuations, thermal behavior across different battery locations, and the activation patterns of electrical contactors responsible for connecting and disconnecting the battery during operation. These outputs are crucial for assessing the battery's performance, identifying potential failure modes, and optimizing its durability and efficiency.

Figures 4.1, 4.2, and 4.3 illustrate the temporal evolution of battery temperature under three distinct driving conditions. Due to confidentiality constraints, the reported graphs do not include a graduated scale. However, the qualitative trends remain evident, highlighting the strong dependence of temperature behavior on driving conditions.

Figure 4.1 corresponds to Profile 1, where the battery experiences alternating temperature slopes. This suggests that the driving pattern associated with Profile 1 involves fluctuating power demands, leading to cyclic heating and cooling effects. In contrast, Figure 4.2 presents Profile 2, in which a temperature decrease is observed during the driving phase. This indicates that the cooling mechanisms, whether active or passive, effectively counteract the heat generation, possibly due to lower power demands or optimized thermal management strategies. Finally, Figure 4.3 depicts Profile 3, where the battery temperature exhibits a continuous increase over time. This behavior implies a high-energy driving scenario, where thermal buildup is predominant and cooling measures are either insufficient or delayed in response to the heat generation.

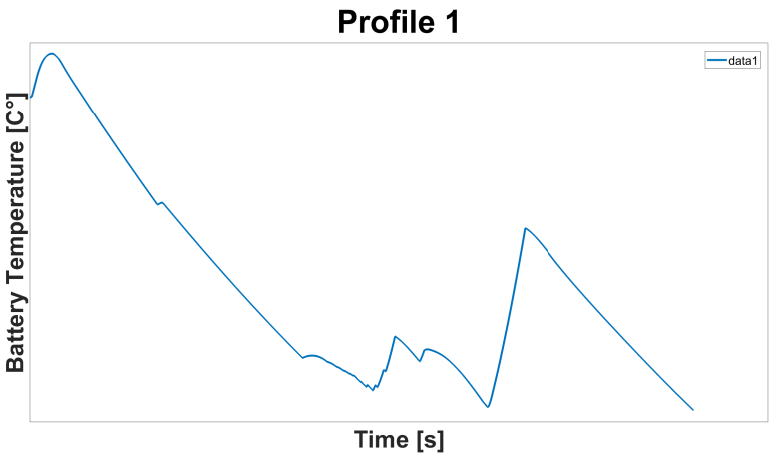

Figure 4.1 Battery temperature response of Profile 1

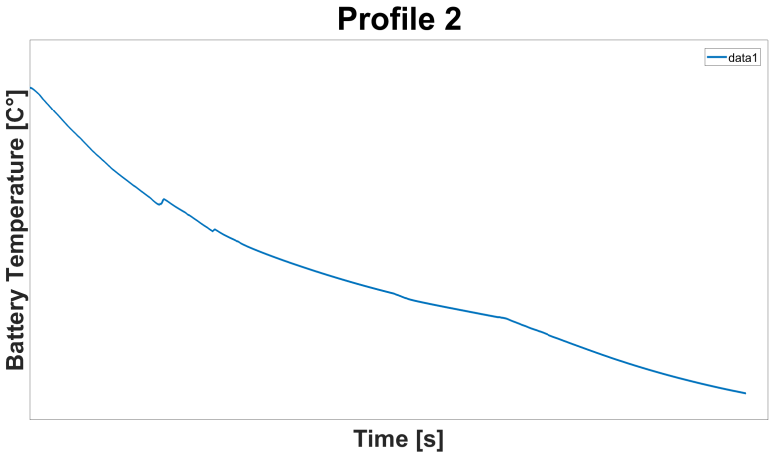

Figure 4.2 Battery temperature response of Profile 2

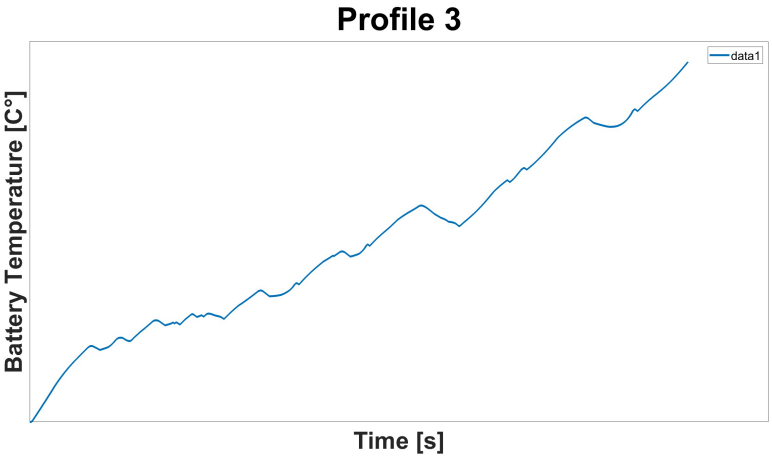

Figure 4.3 Battery temperature response of Profile 3

For the sake of clarity and conciseness, only these three representative driving profiles are presented in this study, despite the fact that a broader range of conditions has been analyzed.

4.4 Cumulated expected Life damage on battery components based on damage model

A MATLAB script is utilized to compute the cumulative damage expected over the life mission of a vehicle. This script is specifically designed to evaluate the damage caused by various failure mechanisms, each of which is associated with a distinct damage model, such as the Coffin-Manson model for fatigue, the Arrhenius equation for thermally activated processes, or the Lawson model for environmental degradation as reported in section 3.2. These models are used to simulate how different operating conditions contribute to the overall degradation of the vehicle's components over time.

The script is structured to operate differently depending on the damage model being analyzed, ensuring that the characteristics of each failure mechanism are properly accounted for. Regardless of the model in use, the analysis follows a systematic process:

1. **Single-Cycle Damage Calculation**: The first step involves calculating the damage produced by a single repetition of a specific operating profile. This calculation takes into account the parameters of the profile, such as temperature, load, and environmental conditions, as well as the specific mathematical formulation of the damage model being applied.

2. **Repetition Scaling**: Once the damage from a single profile repetition is determined, this value is scaled by multiplying it by the number of repetitions expected for that profile during the vehicle's life mission. This step reflects the cumulative impact of repeated stress cycles or environmental exposures that occur over time.

3. **Damage Summation**: After computing the damage for each individual operating profile and accounting for its respective repetition count, the script aggregates the results. The total damage is calculated by summing the contributions from all operating profiles and their repetitions. This summation provides a comprehensive estimate of the cumulative damage experienced by the vehicle's components throughout their operational lifetime.

By following this process, the script effectively combines the damage contributions from multiple failure mechanisms, each governed by its respective model. This allows for a detailed and accurate assessment of the overall durability and reliability of the vehicle under its expected life mission conditions. Such insights are invaluable for identifying potential weak points, optimizing component design, and ensuring the vehicle meets its intended lifespan and performance requirements.

Profile 1 Coffin-Manson damage calculation example. (Single-Cycle Damage Calculation)

As reported in subsection 3.2.1 the number of cycles to failure N_f is determined by the following equation: $N_f = \frac{A}{(\Delta T)^C}$. N_f can be also seen as the number of cycles experienced during the service life at that specific ΔT. Consequently the damage from Coffin Manson model (D_{coffin}) is proportional to the cycles to failure which are proportional the temperature gradient ΔT. The Matlab scripts utilizes a rain-flow counting function to analyze the amplitude and repetitions of the temperature oscillation present in Profile 1.

The rainflow counting technique was introduced in 1968 and was the first accepted method used to extract closed loading reversals or cycles. The therm rainflow refers to the comparison of this method to the flow of rain falling on a pagoda and running down the ages of the roof [64]. Here taking the temperature evolution of Profile 1 in Figure 4.1 the example of counting technique is reported:

- Rotate the loading history of 90 degrees such that the time axis is vertically downward and the load time history resembles a pagoda roof.
- Imagine a flow of rain starting at each successive extremum point.
- Define a loading reversal (half-cycle) to continue to drip down the roof until: it falls opposite to a larger maximum (or smaller minimum) point, it meets a previous flow falling from above or it falls below the roof.
- Identify each cycle by pairing up the same counted reversal.

In Figure 4.4 an approximation of ΔT counting in Profile 1 is reported. It is an approximation because only the temperature oscillations with highest magnitude are reported in Figure 4.4 for simplicity.

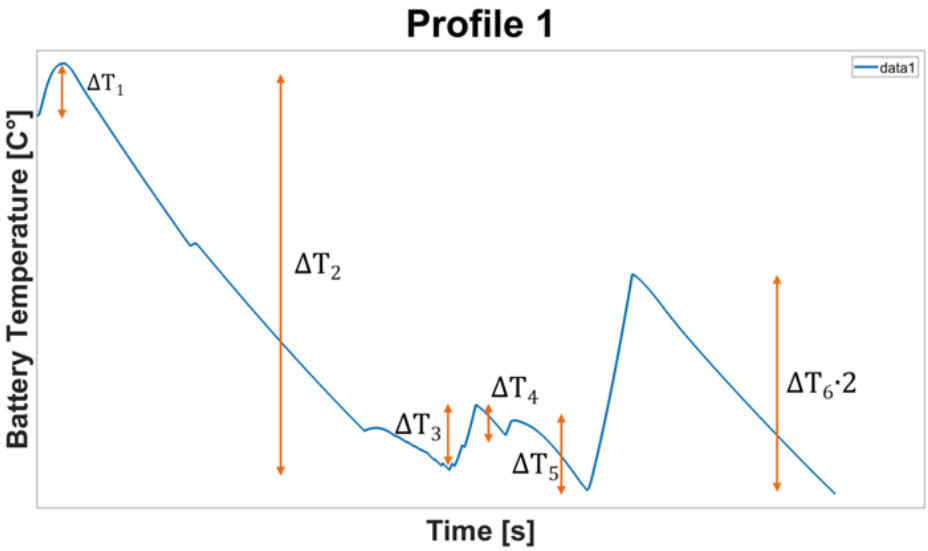

Figure 4.4 ΔT approximation counting of Profile 1 by rainflow method.

4.5 Cumulated expected Accelerated test damage on battery components based on damage model

To evaluate the fatigue damage induced by accelerated test profiles on battery components, the same MATLAB script described in Subsection 4.4 is utilized. However, in this specific analysis, the focus is restricted to a single selected accelerated test profile, rather than considering multiple endurance profiles. The list of available accelerated tests, which are typically conducted, is provided in Subsection 2.5.4.

Once the fatigue damage corresponding to a single test cycle of the chosen profile is computed using the MATLAB script, the total expected damage over the entire test is determined by multiplying the computed single-cycle damage by the total number of test cycle repetitions. This approach allows for an estimation of the cumulative damage that the component experiences throughout the complete test duration.

For demonstration purposes, this subsection presents the computation of fatigue damage for the PTCE (Power-Thermal Cycling Endurance) accelerated test profile. The Coffin-Manson model is employed to assess the fatigue damage due to temperature variations. To facilitate better visualization, the single-cycle profile of the PTCE test is illustrated in Figure 4.5.

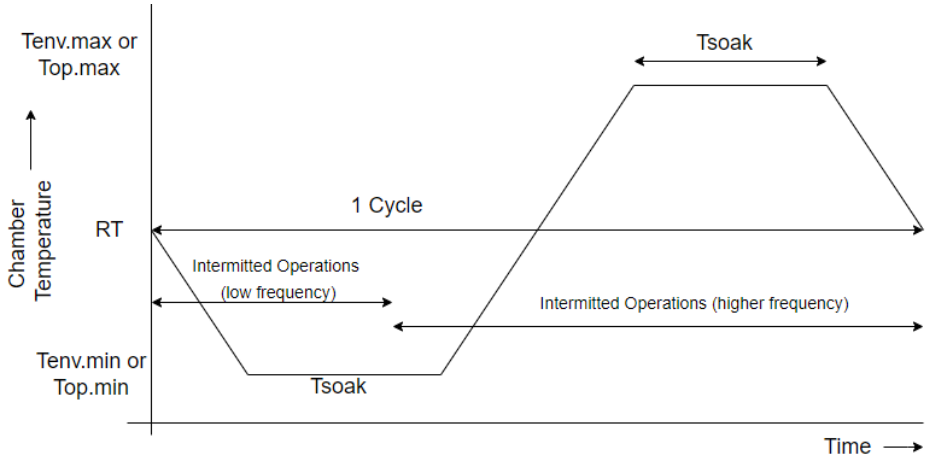

Figure 4.5 Single cycle profile of the PTCE test, showing temperature variations.

As depicted in Figure 4.5, the PTCE test cycle consists of three distinct temperature variations (ΔT):

- The first temperature variation occurs from the reference temperature to the minimum environmental temperature, $T_{env.min}$.
- The second temperature variation takes place from $T_{env.min}$ to the maximum environmental temperature, $T_{env.max}$.
- The third and final temperature variation involves a return from $T_{env.max}$ back to the reference temperature.

The PTCE profile is specifically optimized to induce large temperature variations, thereby maximizing the thermal stress on the battery component under test.

The intention behind this approach is to accelerate the aging and fatigue damage mechanisms, ensuring that the most severe operational conditions are replicated in a controlled testing environment.

In a manner similar to the damage computation for Life Mission Profile 1, the MATLAB script applies the rainflow counting algorithm to identify the distinct temperature oscillations within the test cycle and to quantify their respective occurrences. The rainflow counting technique is essential for determining the cyclic nature of temperature fluctuations and for accurately assessing the fatigue damage accumulation over multiple repetitions of the test cycle.

Once the temperature oscillations and their respective cycle counts are obtained, the script utilizes the Coffin-Manson fatigue damage model to evaluate the effect of the thermal cycling on the battery component. The Coffin-Manson model relates the fatigue damage to the amplitude of thermal cycles and the material properties of the component under test. The total fatigue damage is computed as:

$$D_{total} = N_{cycles} \sum_{i=1}^{n} (\Delta T_i)^c \,, \tag{4.1}$$

where N_{cycles} is the total number of test repetitions, ΔT_i represents the temperature range for each cycle, and m is the Coffin-Manson exponent, which depends on the material properties of the tested component.

By applying this methodology, the expected cumulative fatigue damage for the PTCE test can be estimated, providing insights into the component's durability and performance under accelerated thermal stress conditions.

4.6 Table of Damage with endurance accelerated tests and relative expected damage with respect to vehicle usage

The concept of the Acceleration Factor (AF) is a fundamental parameter used to quantify the ratio of damage experienced by a battery component during accelerated testing cycles in comparison to the damage that would be expected over the entire lifespan of the component under normal operating conditions. This factor plays a crucial role in evaluating the effectiveness of accelerated testing procedures and ensuring that the tests conducted provide a reliable representation of real-life damage accumulation.

Figure 4.6 presents the Table of Damage derived from this study. It serves as a valuable tool in assessing the relationship between the damage expected at various battery locations throughout their operational life and the damage accumulated at the same locations during specific test cycles. The Table of Damage is structured as follows: the first column lists the different damage models that have been analyzed, the second row reports the normalized life mission damage corresponding to each model, and the subsequent columns, from column 3 to column 6, contain the normalized cumulative damage data. These cumulative damage values represent the damage accumulated through multiple endurance tests, normalized with respect to the expected life mission damage for the corresponding damage model.

The cooling plate collector failure location illustrated in sub-chapter 2.1.3, is not part of this matrix due to timing constraint.

Damage Model	Normalized Life Mission	PTCE	Test 2	Test 3	Test4
CoffinManson_tab	1,0	0,9	1,2	2,1	2,34
Arrhenius_tab	1,0	0,1	1,2	2,3	0,19

Figure 4.6 Table of Damage showing the acceleration factor of different test with respect to the Life Mission.

From the Table of Damage, it is evident that in the first row and third column, the acceleration factor is calculated as 0.9. This value corresponds to the application of the PTCE test and its impact on the battery tab, evaluated through the Coffin-Manson damage model. The interpretation of this result indicates that when subjected to the PTCE test, the accumulated damage on the battery tab is lower than the damage that would naturally occur over its operational life span under real-world conditions, as predicted by the Coffin-Manson model. Consequently, using the PTCE test in its current form for reliability assessment could lead to inaccurate conclusions regarding the durability and performance of the battery component. Since the test does not induce sufficient damage relative to real-life scenarios, it fails to adequately replicate operational stresses, thereby limiting its effectiveness in ensuring the reliability of the component.

On the other hand, the Table of Damage also provides insights into an alternative testing approach that would yield a more reliable evaluation of battery reliability. Specifically, when analyzing the *TEST 3* profile in contrast to the PTCE profile, it is observed that the acceleration factor for the failure mode concerning the Tab-Tab welding connection, as assessed by the Coffin-Manson model, exceeds a value of 1.9 across all corresponding matrix cells. This finding suggests that the *TEST 3* profile subjects the component to damage levels significantly higher than those expected throughout its operational life. Such an outcome implies that the *TEST 3* test cycle provides a more accelerated and severe assessment, ensuring that potential failure mechanisms are more effectively captured, leading to a more robust reliability evaluation.

In addition to the Coffin-Manson model, the Table of Damage also reports data concerning the accumulated damage expected in both the life mission and during testing for the battery cell's tab, as assessed using the Arrhenius model. By examining row 3 of the Table of Damage, which corresponds to the Arrhenius_tab damage model, it becomes apparent that the damage accumulated on the tab due to the PTCE test is significantly lower than the damage anticipated under real-world conditions. This discrepancy underscores the necessity of incorporating multiple damage models when assessing reliability to account for different failure mechanisms that may contribute to component degradation.

Notably, rows 1 and 3 of the Table of Damage analyze the same failure mode, namely, the degradation of the Tab-Tab welding connection. However, the Coffin-Manson and Arrhenius models are based on distinct failure mechanisms. The Coffin-Manson model primarily characterizes failure due to thermal expansion fatigue, where damage accumulation is driven by cyclic variations in temperature. In contrast, the Arrhenius model is founded on the principle that prolonged exposure to elevated temperatures accelerates chemical reactions within the materials, lead-

ing to degradation processes such as breakdown, oxidation, and structural weakening. The divergence in acceleration factor values between these two models for the PTCE test applied to the battery tabs is attributed to the different damage inputs considered by each model. While the Coffin-Manson model accounts for temperature amplitude variations as the primary driver of damage, the Arrhenius model emphasizes the effect of sustained high-temperature exposure.

This outcome highlights a crucial consideration in the design of accelerated reliability tests: understanding the fundamental failure mechanisms underlying a given failure mode is essential to developing test protocols capable of distinguishing between multiple contributing factors to failure. A well-structured testing strategy should encompass a comprehensive approach that considers various degradation mechanisms to avoid overlooking critical damage pathways. By incorporating multiple models and ensuring that the testing procedure effectively replicates real-world operating conditions, it becomes possible to enhance the accuracy and reliability of battery component assessments, ultimately contributing to more robust and effective battery designs.

Chapter 5

Conclusion

The research presented in this thesis aimed to investigate battery pack failure modes and optimize test bench performance using a Physics of Failure (PoF) approach. Through an in-depth analysis of lithium-ion batteries (LIBs) degradation mechanisms, including thermal, mechanical, and electrochemical stressors, this study contributes to the broader effort of enhancing battery reliability and safety. The findings highlight the critical role of failure modeling in improving battery design and testing methodologies while reducing costs and development time. As the demand for electric mobility continues to rise, these findings provide a crucial step toward ensuring the long-term durability and sustainability of next-generation battery technologies.

Key Findings

One of the primary contributions of this work is the identification and classification of failure mechanisms affecting LIBs in real-world automotive applications. The study emphasized the impact of thermal runaway, mechanical abuse, electrical abuse, and non-catastrophic failures such as loss of functionality and capacity loss. By utilizing endurance driving profiles across different regions and multiple stress tests, this thesis analyzed operational conditions to assess failure modes and predict the damage of components in life.

The research also demonstrated the efficacy of the Table of Damage approach in refining the testing process. By identifying redundant tests that do not contribute to meaningful insights into battery failures, this study proposes an optimized test protocol. This not only reduces the financial burden of extensive battery testing but also accelerates the validation process for new battery technologies. Additionally, this Table of Damage approach is particularly useful as a process optimization tool, as it computes the relative damage test-life mission in a short time. If a specific test variable during the process changes or if the number of repetitions of a specific profile of the life mission changes, the MATLAB script can quickly provide updated results about the effectiveness of the tests performed to aim reliability in product life, saving both time and money.

Future Work

While this thesis provides valuable insights into battery failure mechanisms and testing optimization, several areas warrant further exploration, including the evaluation of additional failure modes and failure mechanisms to better assess the expected damage life mission-test cycles of more components in the battery.

Extended field data analysis is necessary to incorporate real-world battery degradation data from in-use electric vehicles, which could further validate and refine the proposed failure models. Advanced simulation techniques, such as machine learning algorithms, could improve predictive maintenance and failure forecasting. The integration of new battery chemistries beyond lithium-ion, such as solid-state and sodium-ion batteries, requires further research into their unique failure modes. Additionally, future studies could examine the sustainability implications of optimized battery testing, particularly in reducing energy consumption and waste during validation processes.

Chapter 6

Acknowledgment

I want to express my sincere gratitude to Mr. Prashant Pant and Professor Hamacher for their support and guidance throughout this study. Their expertise and advice have been invaluable in shaping my research.

A huge thank you to my colleagues at the company, who made this journey even more enriching. In particular, I am incredibly grateful to my mentor Irene Donà for believing in my potential and professionalism. Her trust and encouragement have meant a lot to me.

I also want to thank my amazing friends from TUM, you made my time during my master's studies unforgettable, probably the best time of my life so far. The memories, late-night discussions, and shared ideas will always stay with me.

Last but not least, my deepest thanks go to my grandmother Laura, who supported me during my childhood and played a big role in my education, and to my parents, whose love and encouragement have always been my foundation.

This journey wouldn't have been the same without all of you. Thank you!

Bibliography

[1] George E Blomgren. “The development and future of lithium ion batteries”. In: *Journal of The Electrochemical Society* 164.1 (2016), A5019 (cit. on p. 9).

[2] Yih-Shing Duh, Kai Hsuan Lin, and Chen-Shan Kao. “Experimental investigation and visualization on thermal runaway of hard prismatic lithium-ion batteries used in smart phones”. In: *Journal of thermal analysis and calorimetry* 132 (2018), pp. 1677–1692 (cit. on p. 9).

[3] Bruce Dunn, Haresh Kamath, and Jean-Marie Tarascon. “Electrical energy storage for the grid: a battery of choices”. In: *Science* 334.6058 (2011), pp. 928–935 (cit. on p. 9).

[4] Khalil Amine et al. “Nanostructured anode material for high-power battery system in electric vehicles”. In: *Advanced materials* 22.28 (2010), p. 3052 (cit. on p. 10).

[5] J-M Tarascon and Michel Armand. “Issues and challenges facing rechargeable lithium batteries”. In: *nature* 414.6861 (2001), pp. 359–367 (cit. on pp. 10, 11).

[6] Yuqing Chen et al. “A review of lithium-ion battery safety concerns: The issues, strategies, and testing standards”. In: *Journal of Energy Chemistry* 59 (2021), pp. 83–99. ISSN: 20954956. DOI: 10.1016/j.jechem.2020.10.017 (cit. on pp. 10, 22).

[7] ZY Jiang et al. “Rapid prediction method for thermal runaway propagation in battery pack based on lumped thermal resistance network and electric circuit analogy”. In: *Applied Energy* 268 (2020), p. 115007 (cit. on p. 10).

[8] Mahammad A Hannan et al. “State-of-the-art and energy management system of lithium-ion batteries in electric vehicle applications: Issues and recommendations”. In: *Ieee Access* 6 (2018), pp. 19362–19378 (cit. on p. 12).

[9] Yu Miao et al. “Current Li-Ion Battery Technologies in Electric Vehicles and Opportunities for Advancements”. In: *Energies* 12.6 (2019), p. 1074. DOI: \url{10.3390/en12061074} (cit. on p. 12).

[10] Michaelm M Thackeray et al. “Lithium insertion into manganese spinels”. In: *Materials research bulletin* 18.4 (1983), pp. 461–472 (cit. on p. 12).

[11] Iqbal Husain et al. “Electric Drive Technology Trends, Challenges, and Opportunities for Future Electric Vehicles”. In: *Proceedings of the IEEE* 109.6 (2021), pp. 1039–1059. ISSN: 0018-9219. DOI: \url{10.1109/JPROC.2020.3046112} (cit. on p. 12).

[12] Won Joon Yun et al. “Distributed deep reinforcement learning for autonomous aerial eVTOL mobility in drone taxi applications”. In: *ICT Express* 7.1 (2021), pp. 1–4 (cit. on p. 12).

[13] Guang Wu, Xing Zhang, and Zuomin Dong. “Powertrain architectures of electrified vehicles: Review, classification and comparison”. In: *Journal of the Franklin Institute* 352.2 (2015), pp. 425–448. ISSN: 00160032. DOI: 10.1016/j.jfranklin.2014.04.018 (cit. on pp. 13, 14, 16, 17).

[14] John Warner. *3.1 Vehicle and Industry Terms*. 2015. URL: https://app.knovel.com/hotlink/khtml/id:kt00UCJJS4/handbook-lithium-ion/vehicle-industry-terms (cit. on pp. 15, 17, 18).

[15] Robert C Green II, Lingfeng Wang, and Mansoor Alam. “The impact of plug-in hybrid electric vehicles on distribution networks: A review and outlook”. In: *Renewable and sustainable energy reviews* 15.1 (2011), pp. 544–553 (cit. on p. 16).

[16] Gianfranco Pistoia and Boryann Liaw. *Behaviour of lithium-ion batteries in electric vehicles: battery health, performance, safety, and cost*. Springer, 2018 (cit. on pp. 17, 18).

[17] John Warner. *4. Battery Pack Design Criteria and Selection*. 2015. URL: https://app.knovel.com/hotlink/khtml/id:kt00UCJJV1/handbook-lithium-ion/battery-pack-design-criteria (cit. on pp. 18, 19).

[18] Yan Wang, Qing Gao, and Hewu Wang. “Structural design and its thermal management performance for battery modules based on refrigerant cooling method”. In: *International Journal of Energy Research* 45.3 (2021), pp. 3821–3837. ISSN: 0363-907X. DOI: 10.1002/er.6035 (cit. on pp. 18, 20).

[19] Abhishek Das et al. “Weldability and shear strength feasibility study for automotive electric vehicle battery tab interconnects”. In: *Journal of the Brazilian Society of Mechanical Sciences and Engineering* 41 (2019), pp. 1–14 (cit. on p. 20).

[20] Hussein Togun et al. “A critical review on the efficient cooling strategy of batteries of electric vehicles: Advances, challenges, future perspectives”. In: *Renewable and Sustainable Energy Reviews* 203 (2024), p. 114732 (cit. on pp. 20, 21).

[21] Zhonghao Rao et al. “Experimental investigation on thermal management of electric vehicle battery with heat pipe”. In: *Energy Conversion and Management* 65 (2013), pp. 92–97 (cit. on p. 20).

[22] Ming Shen and Qing Gao. “System simulation on refrigerant-based battery thermal management technology for electric vehicles”. In: *Energy Conversion and Management* 203 (2020), p. 112176 (cit. on p. 20).

[23] Elham Sahraei, Joseph Meier, and Tomasz Wierzbicki. “Characterizing and modeling mechanical properties and onset of short circuit for three types of lithium-ion pouch cells”. In: *Journal of Power Sources* 247 (2014), pp. 503–516 (cit. on p. 22).

[24] Donal P Finegan et al. “In-operando high-speed tomography of lithium-ion batteries during thermal runaway”. In: *Nature communications* 6.1 (2015), p. 6924 (cit. on p. 22).

[25] Hui-Fang LI, Jun-Kui GAO, and Shao-Li ZHANG. “Effect of overdischarge on swelling and recharge performance of lithium ion cells”. In: *Chinese journal of chemistry* 26.9 (2008), pp. 1585–1588 (cit. on p. 22).

[26] Sheng Shui Zhang. “A review on electrolyte additives for lithium-ion batteries”. In: *Journal of Power Sources* 162.2 (2006), pp. 1379–1394 (cit. on p. 22).

[27] Zhi Wang et al. “Thermal runaway and fire behaviors of large-scale lithium ion batteries with different heating methods”. In: *Journal of hazardous materials* 379 (2019), p. 120730 (cit. on p. 23).

[28] Todd M Bandhauer, Srinivas Garimella, and Thomas F Fuller. “A critical review of thermal issues in lithium-ion batteries”. In: *Journal of the electrochemical society* 158.3 (2011), R1 (cit. on p. 23).

[29] Wafa Ben Hassen and Mariem Slimani. “Lithium-ion Battery Tab Welding Diagnosis using Electrical Reflectometry”. In: *2024 IEEE AUTOTESTCON*. IEEE, 2024, pp. 1–6. ISBN: 979-8-3503-4943-6. DOI: \url{10.1109/AUTOTESTCON47465.2024.10697527} (cit. on p. 23).

[30] Nanzhu Zhao et al. “A Fatigue Life Study of Ultrasonically Welded Lithium-Ion Battery Tab Joints Based on Electrical Resistance”. In: *Journal of Manufacturing Science and Engineering* 136.5 (2014). ISSN: 1087-1357. DOI: \url{10.1115/1.4027878} (cit. on p. 23).

[31] Tianzhu Sun et al. “Effect of Micro Solidification Crack on Mechanical Performance of Remote Laser Welded AA6063-T6 Fillet Lap Joint in Automotive Battery Tray Construction”. In: *Applied Sciences* 11.10 (2021), p. 4522. DOI: \url{10.3390/app11104522} (cit. on p. 23).

[32] Won Mo Seong et al. “Abnormal self-discharge in lithium-ion batteries”. In: *Energy & Environmental Science* 11.4 (2018), pp. 970–978 (cit. on p. 24).

[33] Paul G. Slade. “Bus Bar Bolted Connections: Reliability and Testing”. In: *2021 IEEE 66th Holm Conference on Electrical Contacts (HLM)*. 2021, pp. 209–216. DOI: 10.1109/HLM51431.2021.9671182 (cit. on p. 24).

[34] “Cyclable Lithium and Capacity Loss in Li-Ion Cells”. In: () (cit. on pp. 24, 25).

[35] Jiagang Xu et al. “Electrode side reactions, capacity loss and mechanical degradation in lithium-ion batteries”. In: *Journal of The Electrochemical Society* 162.10 (2015), A2026 (cit. on p. 25).

[36] Ivo Babuska and J Tinsley Oden. “Verification and validation in computational engineering and science: basic concepts”. In: *Computer methods in applied mechanics and engineering* 193.36-38 (2004), pp. 4057–4066 (cit. on p. 26).

[37] P.G. Maropoulos and D. Ceglarek. “Design verification and validation in product lifecycle”. In: *CIRP Annals* 59.2 (2010), pp. 740–759. ISSN: 0007-8506. DOI: https://doi.org/10.1016/j.cirp.2010.05.005. URL: https://www.sciencedirect.com/science/article/pii/S0007850610001927 (cit. on p. 26).

[38] ProductIP. *How does homologation work?* Accessed: 2025-01-07. 2023. URL: https://www.productip.com/kb/productipedia/compliance-resources/how-does-homologation-work (cit. on p. 28).

[39] TÜV SÜD. *Homologation and Global Market Access*. Accessed: 2025-01-07. 2023. URL: https://www.tuvsud.com/en-us/industries/mobility-and-automotive/automotive-and-oem/homologation-and-global-market-access (cit. on p. 28).

[40] United Nations. "UN Manual of Tests and Criteria, Part III, Sub-section 38.3". In: (2009), pp. 394–401 (cit. on pp. 28–30).

[41] Volkswagen AG. *Volkswagen Werksnorm VW 80000: Electric and Electronic Components in Motor Vehicles up to 3.5 t – General Requirements, Test Conditions, and Tests*. Tech. rep. Germany: Volkswagen AG, 2017 (cit. on pp. 28, 32, 33, 45).

[42] Martin J. Brand et al. "Effects of vibrations and shocks on lithium-ion cells". In: *Journal of Power Sources* 288 (2015), pp. 62–69. ISSN: 03787753. DOI: 10.1016/j.jpowsour.2015.04.107 (cit. on pp. 28, 29).

[43] Daniel Harvey Doughty and Chris C Crafts. *FreedomCAR: electrical energy storage system abuse test manual for electric and hybrid electric vehicle applications.* Tech. rep. Sandia National Laboratories (SNL), Albuquerque, NM, and Livermore, CA . . ., 2006 (cit. on p. 30).

[44] V. Ruiz et al. "A review of international abuse testing standards and regulations for lithium ion batteries in electric and hybrid electric vehicles". In: *Renewable and Sustainable Energy Reviews* 81 (2018), pp. 1427–1452. ISSN: 13640321. DOI: 10.1016/j.rser.2017.05.195 (cit. on p. 30).

[45] E. Cabrera Castillo. "Standards for electric vehicle batteries and associated testing procedures". In: *Advances in Battery Technologies for Electric Vehicles*. Elsevier, 2015, pp. 469–494. ISBN: 9781782423775. DOI: 10.1016/B978-1-78242-377-5.00018-2 (cit. on pp. 30, 31).

[46] Michael A Roscher, Jochen Assfalg, and Oliver S Bohlen. "Detection of utilizable capacity deterioration in battery systems". In: *IEEE Transactions on vehicular technology* 60.1 (2010), pp. 98–103 (cit. on p. 31).

[47] Xuebing Han et al. "A comparative study of commercial lithium ion battery cycle life in electric vehicle: Capacity loss estimation". In: *Journal of Power Sources* 268 (2014), pp. 658–669 (cit. on pp. 31, 32).

[48] Andreas Haspl, Michael Leighton, and Guenter Winkler. "Reduction of Testing Time of PTCE/HTOE Tests Based on Real Road Load Profiles". In: *SAE Technical Paper Series*. SAE Technical Paper Series. SAE International400 Commonwealth Drive, Warrendale, PA, United States, 2022. DOI: \url{10.4271/2022-01-0176} (cit. on p. 32).

[49] Bernd Bertsche. *Reliability in automotive and mechanical engineering: determination of component and system reliability*. Springer Science & Business Media, 2008 (cit. on p. 32).

[50] "ISO 16750-4: 2010; Road vehicles — Environmental conditions and testing for electrical and electronic equipment". In: () (cit. on p. 32).

[51] Test Navi. *One Approach to Accelerated Humidity Testing*. Accessed: 2025-01-14. 2016. URL: https://www.test-navi.com/eng/report/pdf/OneApproachToAcceleratedHumidity.pdf (cit. on pp. 33, 34).

[52] Karl Hauffe. *Oxidation of metals*. Springer Science & Business Media, 2012 (cit. on p. 33).

[53] Abdalla Youssef et al. "Reliability analysis of solder joints under different thermal and thermo-mechanical loading conditions: Case study of automotive ECUs". In: *2016 17th International Conference on Thermal, Mechanical and Multi-Physics Simulation and Experiments in Microelectronics and Microsystems (EuroSimE)*. IEEE, 2016, pp. 1–6. ISBN: 978-1-5090-2106-2. DOI: \url{10.1109/EuroSimE.2016.7463312} (cit. on p. 35).

[54] C. Hendricks et al. "Physics-of-failure (PoF) methodology for electronic reliability". In: *Reliability Characterisation of Electrical and Electronic Systems*. Elsevier, 2015, pp. 27–42. ISBN: 9781782422211. DOI: \url{10.1016/B978-1-78242-221-1.00003-4} (cit. on pp. 37, 38).

[55] Huai Wang et al. "Transitioning to Physics-of-Failure as a Reliability Driver in Power Electronics". In: *IEEE Journal of Emerging and Selected Topics in Power Electronics* 2.1 (2014), pp. 97–114. DOI: 10.1109/JESTPE.2013.2290282 (cit. on p. 37).

[56] J. Hu et al. "Role of Failure-Mechanism Identification in Accelerated Testing". In: *Journal of the IES* 36.4 (Oct. 2006), pp. 39–45. ISSN: 1052-2883. DOI: 10.17764/jiet.2.36.4.b01608702h803nkm. eprint: https://meridian.allenpress.com/jiest/article-pdf/36/4/39/2220787/jiet_2_36_4_b01608702h803nkm.pdf. URL: https://doi.org/10.17764/jiet.2.36.4.b01608702h803nkm (cit. on p. 37).

[57] Pratap Singh and Puligandla Viswanadham. *Failure modes and mechanisms in electronic packages*. Springer Science & Business Media, 1997 (cit. on p. 39).

[58] Luis A. Escobar and William Q. Meeker. "A Review of Accelerated Test Models". In: *Statistical Science* 21.4 (2006). ISSN: 0883-4237. DOI: \url{10.1214/088342306000000321} (cit. on p. 39).

[59] FCA ITALY. "CS.00056. ENVIRONMENTAL SPECIFICATION FOR ELECTRICAL / ELECTRONIC (E/E) COMPONENTS". In: () (cit. on pp. 39–41, 43).

[60] Weiping Diao et al. "Evaluation of Present Accelerated Temperature Testing and Modeling of Batteries". In: *Applied Sciences* 8.10 (2018), p. 1786. DOI: \url{10.3390/app8101786} (cit. on p. 41).

[61] Keith J. Laidler. "The development of the Arrhenius equation". In: () (cit. on p. 41).

[62] Stewart K. Kurtz and D. Stewart Peck. "Microelectronic reliability, vol. II: Integrity assessment and assurance: Edited by Emiliano Pollino. Artech House, Norwood, Massachusetts (1989). Price: $78.00 ISBN 089006 - 350 - 8$". In: *Materials Research Bulletin* 24.11 (1989), pp. 1425–1426. ISSN: 0025-5408. DOI: https://doi.org/10.1016/0025-5408(89)90150-5. URL: https://www.sciencedirect.com/science/article/pii/0025540889901505 (cit. on p. 42).

[63] Cheng Lin, Aihua Tang, and Wenwei Wang. “A Review of SOH Estimation Methods in Lithium-ion Batteries for Electric Vehicle Applications”. In: *Energy Procedia* 75 (2015), pp. 1920–1925. ISSN: 18766102. DOI: 10.1016/j.egypro.2015.07.199 (cit. on pp. 45, 46).

[64] Yung-Li Lee and Tana Tjhung. “Rainflow cycle counting techniques”. In: *Metal Fatigue Analysis Handbook: Practical Problem-solving Techniques for Computer-aided Engineering* 89 (2011) (cit. on p. 51).

Acronyms

AF	Acceleration Factor. 42, 53
ALT	Accelerated Life Testing. 9, 38
BEVs	Battery electric vehicles. 12
BMS	Battery Management System. 17, 23, 24
BTMS	Battery Thermal Management System. 19–21
C	Nominal capacity. 30, 31
DV	Design Validation. 25
EOL	End of Life. 45
EV	Electric Vehicles. 22
EVs	electric vehicles. 11–13
eVTOL	Electric vertical takeoff and landing. 12
HEV	Hybrid Electric Vehicles. 15, 16, 18, 19
HTHE	High Temperature & High Humidity Cycle Test. 33, 34, 43
HTOE	High Temperature Operating Endurance Cycle. 35
LCO	Lithium Cobalt Oxide. 12
LFP	Lithium Iron Phosphate battery. 31
LIBs	Lithium-ion batteries. 9, 10, 21–24, 57
NMC	Lithium Nickel Manganese Cobalt Oxide. 12
OCV	Open Circuit Voltage. 28
Parallel HEV	Parallel Hybrid Electric Vehicles. 13, 15, 16
PEV	Pure Electric Vehicles. 13–15
PHEVs	Plug-in hybrid electric vehicles. 12, 16
PoF	Physics of Failure. 9, 37, 57
PSHEV	Power-split Hybrid Electric Vehicles. 13
PTCE	Power Thermal Cycle Endurance. 32, 33, 40, 52, 53

PV	Process Validation. 25
SEI	Solid Electrolyte Interphase. 24, 25, 41
Series HEV	Series Hybrid Electric Vehicles. 13, 15
SLI	starting, lighting and ignition. 11
SOC	State of Charge. 22, 46
TTF	Time to Failure. 37
VCU	Vehicle Control Unit. 16